Earth's Future

RESEARCH ARTICLE
10.1029/2023EF003663

Special Section:
Quantifying Nature-based Climate Solutions

A Century of Reforestation Reduced Anthropogenic Warming in the Eastern United States

Mallory L. Barnes[1], Quan Zhang[2], Scott M. Robeson[3], Lily Young[1], Elizabeth A. Burakowski[4], A. Christopher. Oishi[5], Paul C. Stoy[6], Gaby Katul[7], and Kimberly A. Novick[1]

[1]O'Neill School of Public and Environmental Affairs, Indiana University, Bloomington, IN, USA, [2]State Key Laboratory of Water Resources and Hydropower Engineering Science, Wuhan University, Wuhan, China, [3]Department of Geography, Indiana University, Bloomington, IN, USA, [4]Institute for the Study of Earth, Oceans, and Space, University of New Hampshire, Durham, NH, USA, [5]Coweeta Hydrologic Laboratory, USDA Forest Service, Southern Research Station, Otto, NC, USA, [6]Department of Biological Systems Engineering, University of Wisconsin–Madison, Madison, WI, USA, [7]Department of Civil and Environmental Engineering, Duke University, Durham, NC, USA

Key Points:

- Reforestation in the eastern United States (EUS) contributes to cooling the land surface and near-surface air temperature
- The biophysical impacts of reforestation help explain the anomalous lack of 20th-century warming in the EUS
- Reforestation in temperate regions can provide biophysical climate adaptation benefits by cooling surface and air temperatures

Supporting Information:

Supporting Information may be found in the online version of this article.

Correspondence to:

M. L. Barnes and K. A. Novick,
malbarn@iu.edu;
knovick@iu.edu

Citation:

Barnes, M. L., Zhang, Q., Robeson, S. M., Young, L., Burakowski, E. A., Oishi, A. C., et al. (2024). A century of reforestation reduced anthropogenic warming in the Eastern United States. *Earth's Future*, *12*, e2023EF003663. https://doi.org/10.1029/2023EF003663

Received 15 MAR 2023
Accepted 7 JAN 2024

Author Contributions:

Conceptualization: Mallory L. Barnes, Scott M. Robeson, Kimberly A. Novick
Data curation: Mallory L. Barnes, Elizabeth A. Burakowski, A. Christopher. Oishi
Formal analysis: Mallory L. Barnes, Quan Zhang, Lily Young, Kimberly A. Novick

Abstract Restoring and preserving the world's forests are promising natural pathways to mitigate some aspects of climate change. In addition to regulating atmospheric carbon dioxide concentrations, forests modify surface and near-surface air temperatures through biophysical processes. In the eastern United States (EUS), widespread reforestation during the 20th century coincided with an anomalous lack of warming, raising questions about reforestation's contribution to local cooling and climate mitigation. Using new cross-scale approaches and multiple independent sources of data, we uncovered links between reforestation and the response of both surface and air temperature in the EUS. Ground- and satellite-based observations showed that EUS forests cool the land surface by 1–2°C annually compared to nearby grasslands and croplands, with the strongest cooling effect during midday in the growing season, when cooling is 2–5°C. Young forests (20–40 years) have the strongest cooling effect on surface temperature. Surface cooling extends to the near-surface air, with forests reducing midday air temperature by up to 1°C compared to nearby non-forests. Analyses of historical land cover and air temperature trends showed that the cooling benefits of reforestation extend across the landscape. Locations surrounded by reforestation were up to 1°C cooler than neighboring locations that did not undergo land cover change, and areas dominated by regrowing forests were associated with cooling temperature trends in much of the EUS. Our work indicates reforestation contributed to the historically slow pace of warming in the EUS, underscoring reforestation's potential as a local climate adaptation strategy in temperate regions.

Plain Language Summary A century of eastern US reforestation has had a cooling effect that helps to explain a lack of regional warming in the 20th century, which stands in contrast to warming trends across the rest of North America during the same period. Our study shows that forests across much of the eastern United States have a substantial adaptive cooling benefit for surface temperature, and for the first time, we demonstrate that this benefit also extends to near-surface air temperature. Therefore, reforestation in temperate zones could provide a complementary set of benefits: mitigating climate change by removing carbon dioxide from the atmosphere, while also helping with adaptation to rising temperatures by cooling surface and air temperatures over large areas.

1. Introduction

Drastic reductions in anthropogenic greenhouse gas emissions are necessary to address climate change. Nature-based Climate Solutions (NbCS), such as reforestation, have the potential to provide additional mitigation through atmospheric CO_2 removal (Nolan et al., 2021; Novick, Metzger, et al., 2022; Novick, Williams, et al., 2022; Seddon et al., 2020), but will only be effective if they are accompanied by economy-wide decarbonization. Changes to land cover and management, which are central to the implementation of NbCS, can alter local temperature through changes to the surface energy balance (Anderson et al., 2011). If these biophysical impacts are beneficial, then some NbCS could serve as a tool for local adaptation in addition to global-scale climate mitigation.

Reforestation—the NbCS with the highest CO_2 mitigation potential (Griscom et al., 2017)—can increase or decrease local surface temperature (T_s) depending on the balance of competing mechanisms. In the tropics, forests

Funding acquisition: Kimberly A. Novick
Investigation: Mallory L. Barnes, Quan Zhang, Scott M. Robeson, Lily Young, Kimberly A. Novick
Methodology: Mallory L. Barnes, Quan Zhang, Lily Young, Paul C. Stoy, Gaby Katul, Kimberly A. Novick
Resources: Kimberly A. Novick
Software: Mallory L. Barnes, Kimberly A. Novick
Validation: Mallory L. Barnes, Kimberly A. Novick
Visualization: Mallory L. Barnes
Writing – original draft: Mallory L. Barnes
Writing – review & editing: Mallory L. Barnes, Quan Zhang, Scott M. Robeson, Elizabeth A. Burakowski, A. Christopher. Oishi, Paul C. Stoy, Gaby Katul, Kimberly A. Novick

evaporate substantially more water than grasslands, which promotes cooling by using energy that would otherwise heat the surface (Anderson et al., 2011; Williams et al., 2021). Conversely, reforestation in boreal climates tends to warm the surface due to both reductions in albedo and the influences of surface roughness on nighttime temperatures (Lee et al., 2011). In the temperate zone, surface cooling from increased evaporative and sensible heat fluxes usually outweighs albedo-driven warming, such that temperate forests have lower T_s compared to non-forested ecosystems (Anderson et al., 2011; Bright et al., 2017; Burakowski et al., 2018; Windisch et al., 2021; Zhang et al., 2020).

Although T_s is relevant to many ecological processes (Farella et al., 2022), the near-surface air temperature (T_a) is an equally important target for climate adaptation (Novick & Katul, 2020; Winckler et al., 2019) because changes in T_a can have far-reaching effects, as biophysical impacts on air temperature can be advected across the landscape (Winckler et al., 2019). While land-cover change affects T_s and T_a differently (Baldocchi & Ma, 2013; Helbig et al., 2021; Novick & Katul, 2020; Winckler et al., 2019), quantifying the impacts of land-cover change on T_a has historically been challenging. Near-surface air temperature cannot be sensed remotely, and its variation with height makes it difficult to interpret over differing land cover types (Novick & Katul, 2020; Winckler et al., 2019). Most data-driven studies investigating biophysical impacts on both T_s and T_a typically compare locations with similar macroclimates but different land cover, which captures the direct, local effects of land-cover change on T_s and T_a (e.g., Baldocchi & Ma, 2013; Bright et al., 2017; Juang et al., 2007; Winckler et al., 2019; Windisch et al., 2021; Zhang et al., 2020). However, this approach can overlook indirect, non-local effects (Baldocchi & Ma, 2013) related to advection or changes in downstream cloud cover due to increased upstream evapotranspiration. This study adopts a novel combination of approaches to evaluate the impacts of reforestation on both T_s and T_a, exploring both local and larger-scale effects across various spatial and temporal scales.

The Eastern United States (EUS) has undergone extensive reforestation over the last century (Figures 1a and 1b; Ramankutty et al., 2010), providing a unique opportunity to investigate the biophysical impacts of large-scale land cover change. By large scales, we mean scales that are sufficiently large so that the atmospheric boundary layer is in local equilibrium with the land-surface. This equilibrium may be achieved at scales much larger (i.e., order of magnitude) than the daytime boundary layer height (order of 1 km). Additionally, the absence of warming over a large portion of the EUS during this period (Figure 1c; Meehl et al., 2012) raises the question of whether reforestation has dampened the historic pace of warming in the region. To address this question, we employ multiple independent data sources to evaluate both local and non-local effects of reforestation on T_s and $T_{a.}$ Our approach involves: (a) comparing locations with similar climates but different land cover using both satellite and in situ observations to determine the local effects of reforestation on T_s and T_a, (b) exploring gradients in T_s across ecosystem boundaries to uncover the potential local extent of such effects, and (c) analyzing historical weather station, air temperature, and land-cover data to identify long-term links between T_a and forest cover trends at landscape and regional scales. Through this comprehensive approach, we aim to gain insight into the extent to which EUS reforestation has influenced historical rates of regional warming and the potential of temperate zone reforestation for climate adaptation.

1.1. Historic Land Cover and Climate Trends in the Region

Before European settlement, forests occupied most of the land area in the EUS, with an uneven-aged stand structure sustained by selective harvest (Novick, Jo, et al., 2022; Ramankutty et al., 2010). However, from the late 18th to early 20th century, forest cover in the EUS dramatically decreased due to harvesting for timber and clearing for agriculture, resulting in forest losses exceeding 90% in some locations (Carman, 2013; Hall et al., 2002; Houghton & Hackler, 2000). By 1930, widespread land clearing had largely stopped, and forest cover began to increase with the abandonment of marginal agricultural fields and active reforestation efforts (Carman, 2013; Hall et al., 2002; Houghton & Hackler, 2000; Ramankutty et al., 2010, and see Figure 1d). Since 1900, millions of hectares of forest have been added in the northeastern, southeastern, and midwestern US (Figure 1b, and Carman, 2013; Hall et al., 2002; Wear & Greis, 2012), mostly through the conversion of crop and pastureland to deciduous forests, or to pine plantations providing softwood timber in some parts of the southeastern US (Wear & Greis, 2012). Many forests in the region are now 50–100 years old (Figure 1a, Figure S1 in Supporting Information S1), although frequent harvest of pine plantations suppresses stand age in the Southeast.

10.1029/2023EF003663

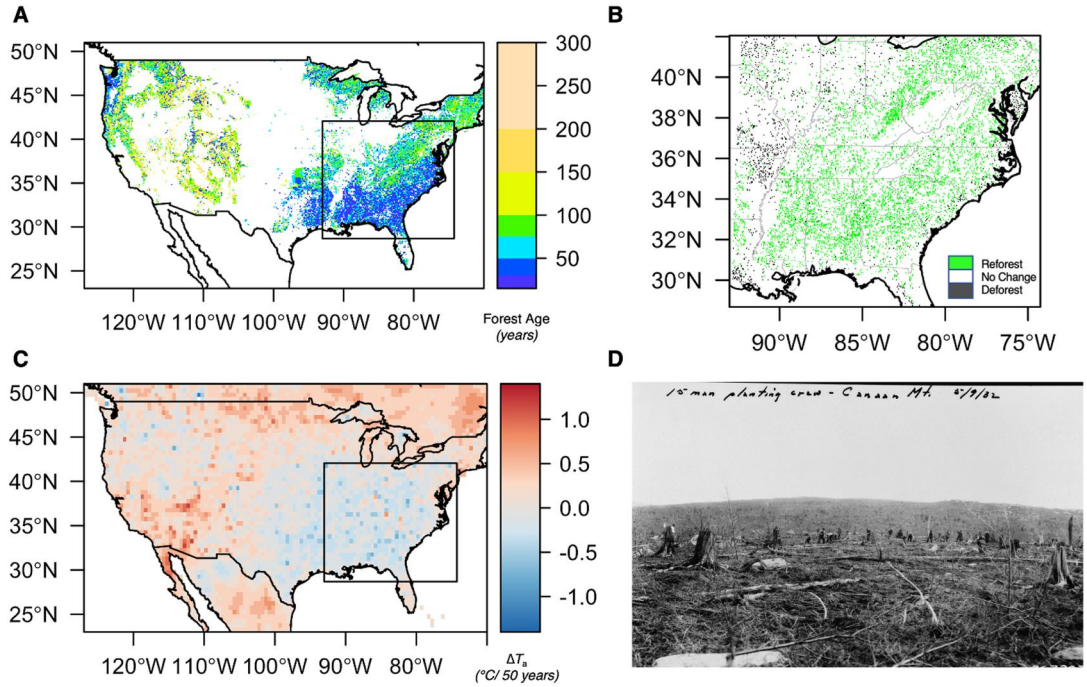

Figure 1. The Southeastern United States' warming hole' and corresponding forest status. (a) Forest age estimates (1 km) as of 2019 calculated from forest age data from the North American Carbon Program. (b) Land conversion between agricultural land and forests from 1938 to 1992 calculated from 1 km FORE-SCE backcasting grids from the US Land Cover Trends project. The bounding box indicates the study area, and details on data sources are provided in the methods. (c) Trend in temperature change from 1900 to 2010 (ΔT_a, °C/50 years) calculated using a season-trend model applied to 0.5° T_a grids from University of Delaware monthly climatologies provided by the NOAA. (d) Historical photo of 15-person planting crew on 05/09/1932 in Tucker County, West Virginia. Original photo at the Forest Service Office in Elinks, WV. Obtained from https://www.loc.gov/pictures/resource/hhh.wv0307.photos.041150p/.

This century of EUS reforestation coincides with an anomalous lack of regional warming, sometimes referred to as a "warming hole" (Figure 1; Mascioli et al., 2017; Meehl et al., 2012; Z. Pan et al., 2004; Partridge et al., 2018; Tosca et al., 2017), especially in the Southeast. While most land areas worldwide warmed during the twentieth century, much of the EUS experienced minor cooling, from −0.2°C to −0.8°C per 50 years (Figure 1c). Proposed explanations for this cooling include internal climate variability (Mascioli et al., 2017; Meehl et al., 2012), anthropogenic aerosols (Tosca et al., 2017), agricultural intensification (Mueller et al., 2016), and increasing precipitation (Z. Pan et al., 2004). However, mechanistic attribution remains elusive (Mascioli et al., 2017; Partridge et al., 2018). The warming hole extends across a large area, predominantly affecting the Eastern and Southeastern US (Figure 1), rather than being confined solely to the Midwest. Previous studies, such as Mueller et al. (2016), have identified local cooling effects on temperature extremes in the Midwest due to agricultural intensification. However, these localized effects on temperature extremes do not fully correspond with the persistent and widespread trends in mean temperatures observed throughout the broader region of the warming hole. Despite the established potential of reforestation to affect local temperature, the impacts of regional reforestation over the past century have not been thoroughly evaluated for their contribution to the "warming hole" in the EUS.

2. Materials and Methods

To evaluate the influence of EUS reforestation on historical warming rates and assess the potential of temperate-zone reforestation as a climate adaptation strategy, we integrated several independent data sources, adopting methods that encompass a range of spatial and temporal scales. Our approaches (outlined in Figure 2) are organized across two axes: biophysical versus historical and local versus regional. In broad terms, our investigation:

1. Analyzes satellite and in situ flux tower observations to quantify the local potential impact of forests, and by extension, reforestation on T_s. We accomplish this analysis by comparing co-located ecosystems with similar

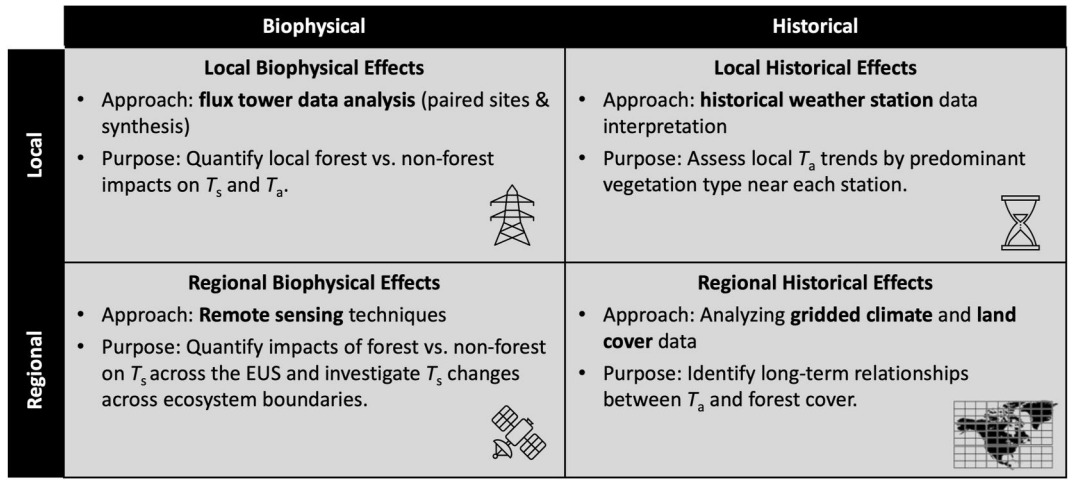

Figure 2. Conceptual representation of the methodological approaches employed in this study. The diagram is divided into four quadrants to differentiate local and regional scales and biophysical and historical contexts. Each quadrant outlines the associated methods and their purpose. The methodologies span a broad range of space (local to regional) and time (diurnal to long-term historical trends) scales and enriches biophysical analyses (energy-radiation balance combined with physiological and aerodynamic approaches) with empirical or data-driven approaches.

climates but different land cover (i.e., paired sites), and). We also utilize a method that normalizes the local T_s time series to account for changes in macro-scale air temperature, enabling us to isolate the land cover effect.

2. Investigates the extent to which changes in T_s extend to near-surface air temperatures at local scales, including across ecosystem boundaries. These analyses leverage eddy-covariance flux data collected at meteorological towers, as well as gradients in satellite-derived T_s across forest-grassland transitions. These approaches help us estimate the potential magnitude and spatial extent of the biophysical effects of reforestation.
3. Integrates historical weather station, climate reanalysis, and land-cover data to trace long-term links between T_a and forest cover at both the local and regional scales. This process involves analyzing the long-term trends in T_a anomalies and determining correlations between forest age and long-term T_a trends.

2.1. Overview of the Relevant Temperature Metrics

Land surface (or skin) temperature (T_s) is commonly used to assess the impacts of land-cover change and is observable from both flux towers and remote sensing platforms. In terrestrial ecosystems, T_s represents the temperature of the uppermost layer of vegetation, reflecting the outcome of the interactive effects of radiative transfer, leaf energy balance, eco-physiological controls on stomatal opening and closure, and aerodynamics. A summary of the temperature metrics employed in this study can be found in Table 1.

T_s is mechanistically connected to near-surface T_a through standard boundary layer theory for stratified turbulent flows. In vegetated systems, a thin layer of air called the roughness sublayer lies between the vegetation and the so-called surface layer (i.e., the layer where the log-law for the mean velocity and mean air temperature profiles hold in near-neutral conditions). For comparative (and conventional) purposes, near-surface T_a is generally measured (and modeled) at a height of 2 m above the surface, but profiles of T_a are influenced by canopy structural

Table 1
Summary and Brief Description of the Relevant Temperature Metrics Used in This Study

Temperature metric	Description
T_s; surface temperature	Temperature at the land surface
T_a; air temperature	Near-surface air temperature
T_{extrap}; extrapolated air temperature	Air temperature extrapolated into the surface layer.
T_{aero}; aerodynamic temperature	Air temperature within the upper reaches of the canopy
$T_{a,Daymet}$; Daymet air temperature	Reference air temperature, not influenced by variability in land cover

effects within the roughness sublayer. In short-stature ecosystems such as grasslands and croplands, the roughness sublayer is typically 1–2 m thick, such that flux tower measurements of T_a are typically made in the surface layer. However, above forests with heights of 10 m or more, the roughness sublayer is much thicker (12–50 m), such that tower T_a indicates the mean air temperature within the roughness sublayer, not the surface layer (Novick & Katul, 2020). Thus, comparing T_a observations across forested and non-forested ecosystems is fraught with potential bias linked to canopy structural effects and measurement height despite the use of a "reference" height of 2 m. To overcome this limitation, we focus on two proxies for T_a that are less impacted by structure effects on the near-surface T_a profile and can therefore be inferred from eddy covariance sensible heat flux tower data, as detailed by Novick & Katul, 2020. The first proxy is the aerodynamic temperature (T_{aero}), which represents the air temperature within the upper reaches of the canopy. The second proxy is the air temperature extrapolated upwards into the lower reach of the surface layer (T_{extrap}).

At the regional scale evaluating the impacts of land cover on T_s requires a strategy to control for background variation in macroclimate. Here, the difference between remotely sensed T_s and gridded T_a was evaluated, with the latter provided by the Daymet (Thornton et al., 2016) product ($T_{a,Daymet}$). Remotely sensed surface temperature is frequently termed "LST" (Land Surface Temperature), but we use T_s here for consistency with the other temperature metrics. Daymet interpolates data from meteorological weather stations, which are typically located over short grass surfaces; therefore, it is viewed here as a "reference" T_a that is not influenced by variability in land cover. Tower-derived estimates of T_s and T_a were also normalized by the DAYMET T_a product, which allowed us to leverage information from all flux towers in the study region, and not just those from co-located paired sites.

2.2. Local Biophysical Analysis

2.2.1. Paired Site Flux Tower Analyses

To mechanistically understand reforestation effects on T_s over the diurnal cycle (i.e., Figures 3c and 3d), a paired site approach (e.g., Lee et al., 2011; Zhang et al., 2020) is used, relying on observations from six forest-grassland site pairs in the study region. The site pairs are in Arkansas, North Carolina (3 pairs), Indiana, and New Hampshire (Table S1 in Supporting Information S1), and each paired set is separated by ~30 km or less. Site descriptions and details on eddy covariance data processing are provided elsewhere (Zhang et al., 2020). Briefly, all data were quality-controlled and gap-filled using community-accepted standards embedded in the REddyProc processing tool (Wutzler et al., 2018). The T_s data were inferred from the outgoing longwave radiation using the Stefan-Boltzmann law, with emissivity estimated as an empirical function of albedo following an established approach (Juang et al., 2007). The attribution of changes in T_s to relevant mechanisms (i.e., variation in sensible vs. latent heat flux) was accomplished through a Taylor-series expansion of the site-level energy balance equation, as described elsewhere (Zhang et al., 2020). In this study, these prior results are aggregated across the site pairs.

The approach to estimate T_{aero} and T_{extrap} is described elsewhere (Novick & Katul, 2020). Briefly, T_{aero} is determined by first quantifying the mean ratio between T_s and the tower-measured T_a when the measured sensible heat flux is near zero, implying that T_a and T_{aero} should be in equilibrium. The determination of tower-measured T_a was performed for each hour of the day at each site separately for the peak of the growing season (June–September) and the dormant season (November-March) and was then used to estimate T_{aero} from the observed T_s for every hourly or half-hourly observation period. The T_{extrap} was then calculated assuming the stability-corrected logarithmic profiles from Monin-Obukhov Similarity Theory (Monin & Obukhov, 1954) hold. Those calculations are forced with the estimated T_{aero} and an estimate for the roughness length for heat that varies as a function of measured friction velocity as well as the momentum roughness length that is presumed constant for fully rough conditions (Novick & Katul, 2020). Here, results are shown for the temperature extrapolated into the first 10 m of the surface layer after conceptually "flattening" the ecosystems by replacing them with a rough surface characterized by two roughness heights: one for momentum absorption and one for heat transfer (see Novick & Katul, 2020 for details and code). This manuscript extends the results presented in Novick and Katul (2020) to the full set of paired sites in Table S1 in Supporting Information S1, noting that Novick and Katul only evaluate the results from the Duke Forest sites in North Carolina.

The T_a data presented in Figure 3 are mean air temperature data measured from a T_a/RH probe (such as the HMP35 or HMP45C, Vaisala) above the canopy, usually at or near the height of the eddy covariance systems (see Table S1 in Supporting Information S1).

10.1029/2023EF003663

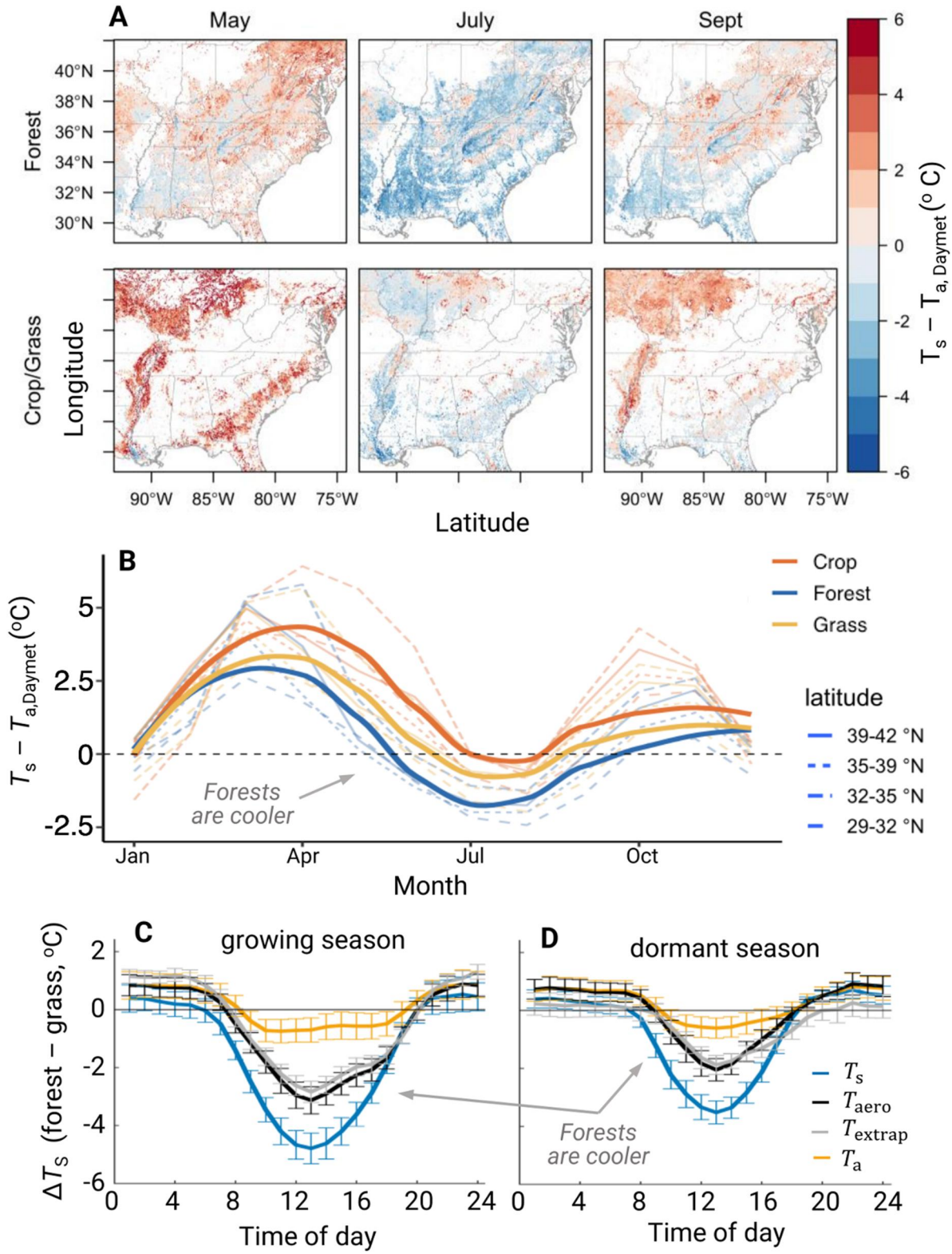

Figure 3.

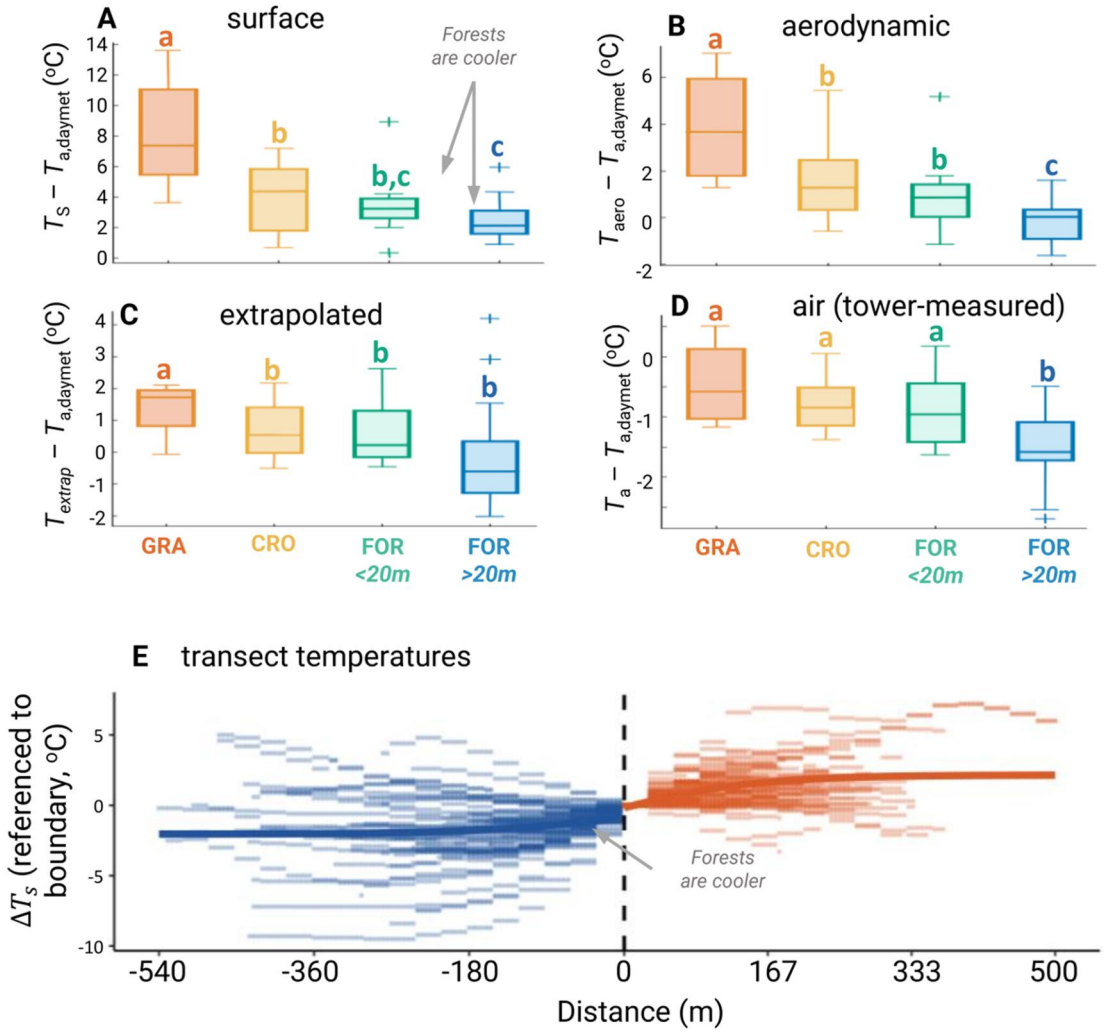

Figure 4. Extension of surface cooling to the near-surface air. (a–d) Difference in tower-measured or derived temperature metrics and reference $T_{a,Daymet}$. Each boxplot shows the monthly midday growing season site-level means, with forested ecosystems split by canopy height (≤20 m or >20 m). Horizontal lines indicate the median, boxes indicate the interquartile range, whiskers indicate the data range (=1.5 times the interquartile range), and the symbols "+" indicate outliers. Letters indicate significant differences between groups evaluated using a two-sample t-test at a significance level of $p = 0.05$. Note the y-axis range varies between panels. Each panel is informed by data from 13 grass towers, 19 cropland towers, 10 towers in forests <20 m *tall*, and 16 towers in forests >20 m tall. (E) Horizontal profiles ("transects") of T_s across the forest:cropland boundary. Values of ΔT_s (sampled every 10 m) are relative to the temperature at the forest:cropland boundary. Negative values of ΔT_s indicate lower temperatures than at the boundary, and positive values of ΔT_s indicate higher temperatures than at the boundary. Points left of the zero-distance line indicate forest (blue), and points right of the zero-distance line indicate agricultural croplands (orange). The blue and orange lines indicate a hyperbolic tangent function fit to the pooled transect data.

2.2.2. Broader Synthesis of Flux Tower Sites

The 58 flux towers used in the broader synthesis (Figures 4a–4d) include the paired tower sites, as well as data sets acquired from the AmeriFlux network (Novick et al., 2018). Specifically included are towers installed and operated by the U.S. National Science Foundation's National Ecological Observatory Network (Metzger

Figure 3. A forest surface cooling effect is evident in both satellite and flux tower (a)–(b) observations (c), (d). (a) Average difference between daily ~1:30 p.m. surface temperature (T_s) and daily maximum air temperature ($T_{a,Daymet}$) for 2003–2018 for forests (top row) and combined grasslands and croplands ("other," second row). Negative values indicate cooler surface than air temperature (surface cooling) and positive values indicate warmer surface air temperature. (b) The seasonal cycle of T_s–$T_{a,Daymet}$ for forests (blue), grasslands (yellow), and croplands (orange) for the study region (bolded lines), with latitude ranges indicated by faint dashed lines. (c), (d) Diurnal time series of the difference between forest and grassland T_s (blue), T_{aero} (black), T_{extrap} (gray), and tower-measured T_a (yellow) for six eddy covariance site pairs (Table S1 in Supporting Information S1) for the growing season (c) and the dormant season (d).

et al., 2019). The network data were limited to those that adopt a CC-BY-4.0 data use license. We first downloaded all available site-years from the network, excluding wetlands and irrigated croplands within the study region. Some sites and site-years were excluded due to missing information about radiative fluxes that are required to derive or calculate the temperature metrics. The towers retained for this analysis are described in Table S2 in Supporting Information S1. The approaches used to determine T_s, T_{aero}, and T_{extrap} for the broader flux synthesis are the same as those described in Section 2.2.1, with the exception that the AmeriFlux data were not gap-filled; rather, data were filtered to exclude those collected under very stable conditions in which turbulence generation is suppressed by buoyancy forces, and to exclude excessively large anomalous observation of sensible heat flux (i.e., >1,000 W/m^2). For the purposes of this paper, croplands managed as corn/soy rotations were treated as separate sites for corn and soy years. Estimates of canopy height and measurement height are required to calculate T_{aero} and T_{extrap}. For most towers, they are available from the AmeriFlux Biological, Ancillary Disturbance, and Metadata (BADM) database. In cases where they were not available from the BADM, they were extracted from published studies. In rare cases, a "best" guess was made based on known information about the canopy type or from site photos.

To synthesize information from this much broader set of flux towers, it is necessary to adjust for the influence of background variation in macro-climate, so the land cover impacts can be isolated. Toward this end, we specifically evaluated the difference between the tower-derived temperature metrics and daily maximum T_a estimates from the gridded 1 km Daymet product (Thornton et al., 2016), referred to as T_s–T_a. During the growing season, vegetated surfaces typically have higher surface temperature than air temperature, and thus a positive T_s–T_a (Mildrexler et al., 2011; Novick & Barnes, 2023). We anticipate a reduced T_s–T_a difference in forests due to their increased transpiration rates due to non-forests, especially at midday when transpiration peaks. This reduced difference reflects the impact of transpiration on sensible heat fluxes and consequently on T_s. To the extent that surface cooling extends to the near-surface air temperature at local scales, we also expect the difference between T_s and T_{aero} and T_{extrap} to be lower for forests than grasslands.

2.3. Regional Biophysical Analysis

2.3.1. Differences in T_s–T_a by Land Cover

To compare relative surface cooling between different types of land cover on a regional scale, we used a remote sensing approach based on T_s retrievals from the Moderate Imaging Resolution Spectroradiometer (MODIS; Wan et al., 2015). These T_s retrievals were adjusted for variation in macroclimate using daily maximum T_a estimates from Daymet (Thornton et al., 2016). The MODIS Land Surface Temperature/Emissivity Daily Product (MYD11A1v6.1) has a spatial resolution of 1 km. The timing of the Aqua MODIS overpass (~1:30 p.m. local time) generally corresponds to the timing of daily maximum T_s estimated from tower measurements (Figure S2 in Supporting Information S1). Thus, to evaluate spatial variability in the difference between remotely sensed T_s, we normalized for macro-scale climate variability by subtracting the daily maximum $T_{a,Daymet}$ from MODIS T_s.

The average T_s–$T_{a,Daymet}$ for each 1 km pixel in the study area was obtained for each month from 2002 to 2018. The data presented in Figures 3a and 3b are the average monthly T_s–$T_{a,Daymet}$ for the full time-series. The land cover type for each 1 km MODIS pixel was determined using the U.S. Geological Survey North American Land-Cover Characteristics 1 km grid-spacing data set, created by the National Center for Earth Resources Observation and Science (EROS) as part of the Global Land Cover Characterization Project (EROS, 2017). This data set, derived from 1 km Advanced Very High-Resolution Radiometer data collected between 1992 and 1993, follows the methodologies described in Loveland et al. (1999). There were relatively few pixels classified as grassland, so we combined croplands and grasslands for the spatial T_s–$T_{a,\ Daymet}$ maps in Figure 3a (see also Figures S3–S5 in Supporting Information S1).

2.3.2. Land Surface Temperature Across Forest/Agriculture Boundaries

The National Land Cover Database (NLCD) land cover data set for 2016 (Dewitz, 2019) was used to identify areas with adjacent forest-agriculture boundaries with a continuous extent of land cover on either side of the boundary. Transects were created across boundaries in the east/west direction at a ~90° angle. The transects were approximately 1 km long (i.e., commensurate with the boundary layer height), with points every 10 m. In total, 44 transects were created in the study area (Figure S6 in Supporting Information S1). We then extracted T_s values from mid-summer clear-sky scenes, all of which were from summer 2018, from the Landsat Provisional Surface

Temperature Product (Cook, 2014; Cook et al., 2014). Only one T_s spatial profile was extracted for each transect, even if multiple images were available. The spatial resolution of Landsat imagery is 30 m, so the 10 m transects include several points within the same pixel. A smooth transition suggests that biophysical feedbacks on T_s are likely linked to T_a through advection and the formation of an internal boundary layer (Hsieh & Katul, 2009), since the surface itself is not mixed. For the lines in Figure 4e, we used a hyperbolic tangent function fit to each side of the transects (forest and agriculture). Distances were scaled from—π to π for fitting, then back-transformed for plotting.

2.4. Local Historical Analysis

2.4.1. Impacts of Reforestation on Air Temperature Trends

To investigate the impact of local land-cover change on long-term air temperature trends, we used monthly air temperature data from 398 United States Historical Climate Network (USHCN) meteorological stations. Meteorological stations, which were relatively evenly distributed across the study area (Figure S7 in Supporting Information S1), allow us to associate locations with their land cover type compared to gridded temperature data. We evaluated the effects of land cover on annual temperature trends from 1900 to 2010 by focusing on both maximum temperatures during the growing season (June, July, August) and annual average temperatures. We did not conduct any interpolation of missing values.

We classified the weather stations based on the predominant land cover within a 500 m circular buffer surrounding each station, using 250 m FORE-SCE (FOREcasting SCEnarios of Land-use Change) backcasting grids from the US Land Cover Trends project (Sohl et al., 2007). This buffer size was chosen after preliminary investigation that suggested the cooler surface T_s of forests could influence T_a of nearby non-forest up to this range. This early assessment was subsequently refined and is presented in Figure 4e. A sensitivity analysis of the influence of different buffer sizes on temperature trends (from 100 to 1,200 m) supported the choice of a 500 m buffer, which optimally balanced capturing the impacts of reforestation on air temperature with minimizing confounding effects of unrelated processes (Figure S8 in Supporting Information S1).

The classification was based on three time points within the range of available data (annual from 1938 to 1992), 1938, 1965, and 1992. The intermediate year, 1965, helped exclude sites that had undergone multiple conversions throughout the 20th century. Pixels were categorized as reforestation areas (change from agriculture to forest) under two conditions: (a) if they were agricultural in 1938, converted to forest cover by 1965, and remained forested in 1992; or (b) they were agricultural in both 1938 and 1965, and then transitioned to forest by 1992. The areas predominantly surrounded by agriculture-to-forest conversion within 500 m of the weather stations were defined as "reforest" sites. Here, "predominant" land cover change refers to the land cover type with the greatest cumulative area, determined by summing the weights of each land cover type within the 500-m buffer. Out of the 398 USHCN stations, 132 were predominantly surrounded by forest, 196 by agriculture, and 22 by reforestation. The remaining 48 sites were excluded due to multiple land cover transitions or deforestation in the 20th century.

To explore the impacts of reforestation on air temperature trends, we compared USHCN sites predominantly surrounded by reforestation to sites where the land cover remained stable as either agriculture or forest ("non-reforest") within a 50 km radius of the "reforested" site. For each year, we calculated the temperature difference between the reforest site and non-reforest site (or sites) within the 50 km buffer. This approach builds upon the paired-site flux tower analyses described in Section 2.2.1 by extending our understanding of the effects of reforestation on surface temperature to near-surface air temperature, covering a much longer period (back to the early 20th century), and including many more site "pairs." Our comparison of neighboring reforested and non-reforested site pairs included analysis of both growing-season maximum temperatures and average annual temperatures. We excluded sites that had more than 5 years of missing data from 1900 to 2010. We had a total of 22 reforest sites and 44 non-reforest sites within 50 km of the reforest sites, resulting in 44 comparisons for annual average data and 42 comparisons for growing season data. The lower number of growing season comparisons is due to missing data for two sites. The reforest sites had a median of two non-reforest sites within a 50 km radius. We based the 50 km radius on a previous study that showed changes in maximum air temperature up to 50 km away from the site of land cover change (Cohn et al., 2019).

2.5. Regional Historical Analysis

2.5.1. Forest Age and Land-Cover Change Analyses

Monthly T_a timeseries with a spatial resolution of 0.5° were obtained from the University of Delaware Air Temperature & Precipitation Data set (Willmott & Matsuura, 2015) provided by the National Oceanic and Atmospheric Administration's Oceanic and Atmospheric Research Earth System Research Laboratory Physical Sciences Division (NOAA/OAR/ESRL PSD), in Boulder, Colorado, USA, from https://psl.noaa.gov. The gridded data are interpolated weather station data (Willmott & Matsuura, 1995), primarily from GHCN2 (Global Historical Climatology Network) observations and the GSOD (Global Surface Summary of Day) archive. Monthly mean air temperature from V4.01 of the University of Delaware Air Temperature & Precipitation Data set was used to assess observed long-term changes in T_a across the continental United States. Per-pixel temperature change in T_a was estimated using a season-trend model (function "STM") in the "greenbrown" package (Forkel & Wutzler, 2015) for R (R Core Team, 2020). The season-trend model in "greenbrown" is based on the additive decomposition model described elsewhere (Verbesselt et al., 2010, 2012). Harmonic and linear terms are used to model seasonal variation and trend, respectively, effectively "detrending" the time series in a single step (Verbesselt et al., 2012).

To assess forest age, we obtained continental forest age maps from the North American Carbon Program (NACP), produced for the year 2006 (Y. Pan et al., 2012). Data were updated to provide forest ages for 2019 by adding 13 years to all forest ages. This approach assumes that all forests continued to regrow and were not cut between 2006 (when the product was produced) and 2019. Although there are certainly locations for which this assumption will not hold, they generally represent a small fraction of the land surface and are mostly contained in the southeastern US where pine plantations are routinely harvested and replanted (Carman, 2013; Figure S1 in Supporting Information S1). Furthermore, this method does not account for disturbances such as fires or insect infestations that could have affected stand age. Nonetheless, the low standard deviations of forest ages—corresponding to the 2006 age map and typically around 10 years (Figure S1C in Supporting Information S1)—suggest a disturbance regime with limited spatial heterogeneity. Recent studies corroborate that forest loss in this region is predominantly not due to fires (Hansen et al., 2013; Tyukavina et al., 2022; van Wees et al., 2021). In the 20th century, fire frequency in the Eastern United States was substantially reduced when compared to frequencies before European settlement (Nowacki & Abrams, 2008).

To assess change in forest status (Figure 1b), land-cover change between 1938 and 1992 was calculated from 250 m FORE-SCE backcasting grids described in Section 2.4.1. Pixels were coded based on their land cover (cropland or forest), and per-pixel change was calculated between 1938 and 1992. To exclude sites that had undergone multiple conversions in the 20th century, an intermediate year, 1965, was also used. Pixels were classified into three categories: reforestation (change from cropland to forest), deforestation (forest to cropland), or "no change" (land cover type was consistent in 1938, 1965, and 1992).

2.5.2. Exploring the Links Between Forest Age and Air Temperature Change

To further investigate the influence of reforestation with a focus on the warming hole, we examined the relation between forest age and recent growing season trends in T_a at the regional scale (Figure 5d). To align the recent "snapshot" of forest age with T_a, we compared the 1 km NACP-derived forest age maps with recent trends (1970–2017) in T_a from the University of Delaware climatologies (Willmott & Matsuura, 2015). We used the season-trend approach described in Section 2.5.1 to estimate the slope of trends in annual T_a time-series from 1970 to 2017 (Figure 5d). The slope of the temperature change from 1970 to 2017, ΔT_a, was calculated for each pixel, and forest age data were aggregated to the coarser 0.5-degree scale of the T_a data (Figure S1B in Supporting Information S1) using a mode function, "modal," in the "raster" R package (Hijmans, 2021), and then resampled using nearest neighbor interpolation. Then, we calculated focal correlations between aggregated forest age (Figure S1B in Supporting Information S1) and temperature trends, specifically, a moving window correlation between ΔT_a from 1970-present and forest age in a 5×5 window using the "raster correlation" function in the "SpatialEco" R package (Evans, 2021).

We note that although gridded daily microscale (1 km) T_a products such as Daymet should be relatively insensitive to local impacts of land cover on T_a (Figure S9 in Supporting Information S1), the fingerprint of reforestation may be detectable from coarser yearly mesoscale T_a estimates at 0.5-degree resolution. Observational and

10.1029/2023EF003663

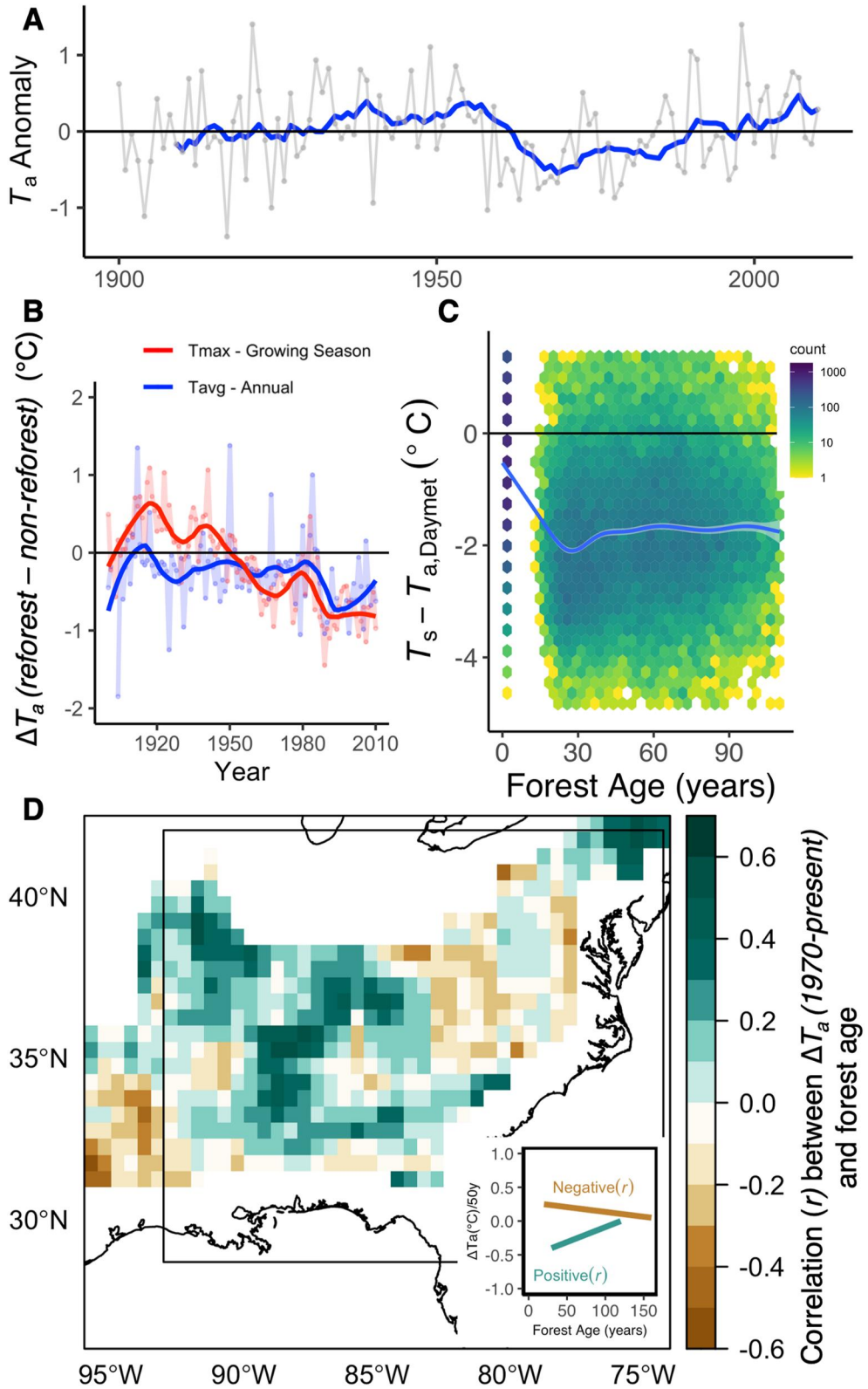

Figure 5.

modeling studies support regional-scale impacts of land cover change on mesoscale T_a (Bonan, 2001; Mahmood et al., 2014), providing further justification for our approach.

3. Results

3.1. Effects of Land Cover on T_s: Local and Regional Biophysical Analysis

Across the study area, the difference between T_s and the $T_{a,Daymet}$ was more negative for forests than grasslands and croplands most of the time (Figure 3). Since the $T_{a,\ Daymet}$ normalizes for macro-scale temperature variability, this result implies that forest surfaces are cooler than the surfaces of nearby grasslands and croplands by the same amount. The effect was most pronounced during the growing season, when forests were cooler than non-forests by 0.6–2.5°C (Figures 3a and 3b), with smaller reductions observed in spring and fall.

Next, we leveraged rich surface energy balance information from eddy covariance flux towers, beginning with six co-located ("paired") forest and grassland sites in the study region (Table S1 in Supporting Information S1; Zhang et al., 2020). Across these paired sites, forest T_s was 4–5°C cooler, on average, than nearby grasslands during midday periods (Figures 3c and 3d), driven primarily by enhanced evapotranspiration in summer and enhanced sensible heat flux in winter that outweighed albedo-driven warming effects in the darker forests (Zhang et al., 2020).

Although the paired-site approach is well established for understanding the biophysical impacts of land-cover change (Zhang et al., 2020), only a handful of forest-grassland flux tower pairs exist. To expand the scope of inference, we synthesized T_s observations from 58 Ameriflux EC tower sites across the EUS, again correcting for macro-scale climate variability with $T_{a,Daymet}$ (Table S2 in Supporting Information S1). The results revealed widespread daytime surface cooling in forests compared to non-forests (Figure 4a). Throughout the growing season, the mean difference between the tower-derived T_s and the reference $T_{a,Daymet}$ was 5.7°C lower for tall (>20 m) forests compared to grasslands, and 4.6°C lower for short (<20 m) forests relative to grasslands (Figure 4a). When comparing forests to croplands, the differences were less pronounced, though tall (>20 m) forests were still relatively cooler than croplands. Specifically, T_s (Figure 4a) was 8.1 ± 3.4 for grasslands, 4.1 ± 2.2 for croplands, 3.5 ± 2.1 for short forests, and 2.4 ± 1.3 for tall forests (all values are mean ± SD).

3.2. Effects of Land Cover on Near-Surface T_a: Local and Regional Biophysical Analysis

For the surface cooling to extend beyond the stand-scale and thus contribute to the warming hole, changes in T_s must translate to changes in near-surface T_a.

We adopted several new or emerging approaches to quantify the extent to which the forest cooling effects on T_s extend to T_a. First, we harnessed flux tower data to estimate metrics of T_a that are less sensitive to canopy effects (Novick & Katul, 2020): T_{aero} and T_{extrap} (Table 1). In the paired sites and across the regional network of flux towers, the midday growing season T_{aero} and T_{extrap} were cooler for forests than for grasslands (Figures 3d, 3e, and 4a–4d).

Consistent with expectations, forests had the strongest cooling effect on surface temperatures (Figure 4a), and smaller effects on air temperatures (Figures 4b–4d). When analyzing the air temperature metrics, T_{aero} and T_{extrap} were similar between forests and croplands, although T_{aero} was substantially lower for tall forest stands (Figure 4b). T_{aero} (Figure 4b) was observed to be 3.9 ± 2.1 for grasslands, 1.5 ± 1.6 for croplands, 1 ± 1.6 for short forests, and notably, −0.2 ± 0.9 for tall forests. Similarly, T_{extrap} (Figure 4c) was 1.3 ± 0.8 for grasslands,

Figure 5. Impact of land cover and forest age on long-term temperature trends. (a) Average trend in pooled annual T_a anomalies for 398 USHCN sites in the EUS. The blue line denotes the 10-year moving average. (b) Difference in T_a between reforested and non-reforested USCHN sites within a 50 km radius. Red and blue lines depict smoothed summer maximum and annual average temperatures, respectively. Negative values indicate cooler temperatures at the reforesting site than its neighboring non-reforesting site(s). (c) July temperature difference (T_s–$T_{a,Daymet}$) versus forest age, using data from 30,000 randomly selected MODIS pixels across the study area. The blue line represents the Generalized Additive Model smooth function, while the surrounding white area depicts its 99% confidence interval. (d) Spatial moving window correlation (5 × 5 window) between forest age and recent long-term T_a trends (1970–2017). A negative correlation indicates older forests are associated with greater cooling, and a positive correlation indicates younger forests are associated with greater cooling (inset).

0.6 ± 0.84 for croplands, 0.6 ± 1 for short forests, and -0.1 ± 1.8 for tall forests. T_{extrap} results showed tall forests to be 1.4°C cooler than grasslands, and short forests were 0.7°C cooler.

Despite the confounding influence of canopy effects on near-surface T_a profiles, tower-measured T_a also suggests a cooling effect of forests, although differences across biomes were smaller (Figure 4d). The mean of the difference between T_s and tower-measured T_a was -0.5 ± 0.7 for grasslands, -0.8 ± 0.4 for croplands, -0.9 ± 0.6 for short forests, and -1.5 ± 0.6 for tall forests. Throughout the growing season, the mean difference between the tower-derived T_s and the tower-measured T_a was 1°C cooler for tall forests compared to grasslands, and 0.7°C cooler for tall forests relative to croplands (Figure 4d).

Next, to provide an independent perspective on surface and air temperature coupling, we used high-resolution (30 m) Landsat T_s retrievals to evaluate the extent to which transitions in T_s at forest-cropland boundaries were smooth or abrupt (Figure 4e; Figure S6 in Supporting Information S1). A relatively smooth temperature transition from cooler forests to warmer croplands was observed (Figure 4e) that extends over length scales of several hundred meters.

3.3. Long-Term Meteorological Observations and Signatures of Land-Cover Change: Local and Regional Historical Analysis

To evaluate the signatures of land-cover change in long-term meteorological observations, we compared long-term records of air temperature from weather station sites, estimates of forest age, and gridded air temperature data (see methods Section 2.4.1). First, long-term temperature trends from 398 USHCN sites in the study region were examined. The examination showed that temperatures remained relatively stable throughout the 20th century, with a decline in average temperatures in the late 1950s (Figure 5a). Next, we investigated the cooling effect of regrowing forests by analyzing the difference between T_s and the reference $T_{a,Daymet}$ as a function of forest age. Results indicated that the cooling effect was strongest for forests around 20–40 years old, as the difference reached its lowest point at that age (Figure 5c).

To further explore the cooling effect of reforestation, we compared 10-year rolling means of T_a from historical USHCN stations in sites predominantly surrounded by reforestation ("reforest") and neighboring sites that did not undergo land cover conversion ("non-reforest") within 50 km. In terms of average annual temperatures, reforested sites were consistently cooler than their non-reforesting counterparts throughout the 20th century (Figure 5b, blue line). The results were more nuanced for maximum growing season temperatures. Sites with nearby reforestation tended to be warmer in the early half of the 20th century and cooler in the latter half, and the magnitude of this cooling effect increased throughout the study period. By the end of the 20th century, reforesting sites were up to 1°C cooler than their non-reforesting neighbors in terms of maximum growing season air temperatures (Figure 5b, red line).

Finally, to explore the relation between forest age and temperature trends, we explored spatial variation in the correlation between decadal-scale growing season T_a trends (from University of Delaware 0.5° monthly climatologies) and forest age across the continental US (Figure 5d). A positive correlation coefficient indicates that pixels dominated by younger forests (i.e., <100 years as of 2019) experienced less warming during this period than pixels dominated by more mature stands (see inset to Figure 5d). This correlation coefficient was positive across much of the study region on the annual timescale (63% of pixels; Figure 5d), and when considering growing season temperature trends alone (Figure S10B in Supporting Information S1), consistent with the expectation that reforesting areas experience less warming. However, there is substantial variability across the study region, with negative relations between forest age and ΔT_a observed, including in the central Appalachians and Ozarks.

4. Discussion

The study provides compelling evidence of the biophysical climate benefits of reforestation in the EUS, while also establishing a clear relation between land-cover changes and temperature shifts observed throughout the 20th century. Taken together, these findings indicate reforestation has a cooling effect on surface and near-surface air temperature in the EUS, and likely contributed to the slower pace of warming in the region. Both ground- and satellite-based observations indicate that EUS forests cool the land surface by 1–2°C annually (Figure 3) compared to nearby surfaces with short-stature vegetation. During midday in the growing season, surface cooling

is 2–5°C (Figures 3c and 4a), and forests aged 25–50 years exhibit the strongest cooling effect (Figure 5c). The surface cooling extends to the near-surface air, with forests reducing midday growing-season air temperature by up to 1°C (Figures 4d and 5b). Historical weather station data and regional-scale gridded long-term air temperature data analyses establish a link between reforestation and the observed lack of warming in the EUS (Figure 5). Weather stations located near reforesting areas recorded temperatures that were 0.5–1.0°C cooler than stations surrounded by land that experienced little change in forest cover. Overall, these results highlight the substantial adaptation potential of reforestation as a nature-based climate solution.

However, these findings may not be applicable across all temperate regions or for all strategies, such as afforestation. The implementation of NbCS must be undertaken with consideration to avoid unintended consequences that could lead to net warming (Novick, Metzger, et al., 2022; Peng et al., 2014). For instance, while reforestation in boreal regions may seem beneficial, changes in albedo and evaporation dynamics could lead to warming in the long-term (Liu et al., 2019; Randerson et al., 2006). Moreover, potential disturbances—such as climatic stressors, wildfires, and insects—carry substantial implications for the success of NbCS. These disturbances could compromise forest carbon storage (Anderegg et al., 2022, particularly in regions more susceptible to these risks like the Western United States), even in regions such as the Eastern United States where these are historically less prevalent. Although forests in the EUS are generally less prone to such disturbances compared to those in the West (Barbero et al., 2015; Bentz et al., 2010), it is nonetheless important to recognize these risks when evaluating region-specific NbCS potential.

4.1. Assessing Land Cover Impacts on Surface and Near-Surface Air Temperature

Assessing the direct consequence of land-cover change on surface temperature is less ambiguous, given the abundance of satellite observations of T_s and complementary measurements of surface energy fluxes from ground-based towers. We have known for some time that reforestation tends to increase T_s in the boreal zone (Bright et al., 2017; Lee et al., 2011; Swann et al., 2010) and decreases T_s in the tropics (Bonan, 2008). In this study of temperate ecosystems, we demonstrated that forests in mid-latitude of the eastern US can contribute to a T_s reduction of 2–5°C at midday during the growing season (Figures 3 and 4a). Furthermore, these reductions in T_s can be achieved within approximately 20 years of forest regeneration (Figure 5c) and remain stable across mature forest classes (Figure 4a). Our findings, combined with other recent work on the topic, contribute to a growing consensus that the presence of forests tends to have a direct cooling effect on T_s across much of the temperate zone.

Remote sensing data inherently favor clear-sky conditions, introducing potential bias into the results presented in Figures 3a and 3b. This bias, however, is mitigated considerably by conducting similar comparisons with flux data (Figure 4a), which are not subject to these clear-sky limitations. Another potential source of bias is associated with the timing of the MODIS overpass. Satellite retrievals are obtained at approximately 1:30 p.m. local time, which could be earlier than when Daymet would record the daily maximum air temperature, particularly in summer. This mismatch might cause the difference between T_s and the Daymet T_a to be lower than it would be in the absence of a temporal discrepancy. Our study, however, primarily focused on comparing the T_s–T_a difference for forested and non-forested areas. Consequently, even if the timing of the MODIS overpass does not align with the peak daily temperatures estimated by Daymet, any small discrepancy would largely be removed when analyzing their difference. Further supporting this point, we found differences in T_s–T_a between forest and non-forest flux sites (Figure 4a) of magnitudes similar magnitude to those from derived from the remote sensing data. These complementary findings lend further credence to our comparative analysis between forested and non-forested areas, thereby strengthening our confidence in the overall results, despite the potential sources of bias.

Assessing the impact of land cover change on near-surface air temperature is more challenging due to technical and methodological limitations. Yet, understanding the potential of reforestation and other natural climate solutions to confer climate adaptation benefits requires that we quantify land cover impacts on near-surface air temperature. Furthermore, for the surface cooling to extend beyond the stand scale and thus contribute to the warming hole, changes in T_s must translate to changes in T_a. In turn, evaluating the impacts of land cover on near-surface air temperatures requires overcoming technical and methodological challenges, including data scarcity and canopy structural effects that prevent straightforward comparisons of air temperature measured above different ecosystems. We adopted several new or emerging approaches to overcome the technical and methodological challenges associated with evaluating T_a.

First, we harnessed flux tower data to estimate metrics of T_a that are less sensitive to canopy effects. By relying on proxies for near-surface air temperature that are relatively insensitive to canopy structural effects (e.g., T_{aero} and T_{extrap}), we demonstrate that, across much of the study region, the cooling effect of forests on T_s extends to the near-surface air temperature above the canopy (Figures 3c and 3d; Figure 4). Forest cover impacts on T_a are smaller than impacts on T_s (~1°C for midday growing season periods, Figures 3d and 4) but still consequential, particularly compared to the magnitude of historic and predicted changes in T_a due to climate change.

Next, to provide an independent perspective on surface and air temperature coupling, we used high-resolution (30 m) Landsat T_s retrievals to evaluate the extent to which transitions in T_s at forest-cropland boundaries were smooth or abrupt. A smoother transition suggests that biophysical feedbacks on T_s are linked to T_a through the formation of an internal boundary layer, assuming the thermal inertia of leaves is small. A relatively smooth temperature transition from cooler forests to warmer croplands was observed (Figure 4e) that extends over length scales typical of adjustment distances needed for the equilibration of the air temperature internal boundary layer. Furthermore, the smooth transition of T_s across forest-grassland boundaries implies coupling between T_s and T_a that extends at least several hundred meters beyond the ecosystem boundary. This result helps to confirm previous theoretical modeling (Hsieh & Katul, 2009; Li & Wang, 2019) and augments a similar exercise in the tropics (Cohn et al., 2019) by documenting these processes at a large spatial scale over much of the EUS. Importantly, it is over this distance that biophysical impacts on T_a are substantial enough to feedback on T_s. It is likely that reforestation impacts on T_a extend further, but beyond a few hundred meters are not great enough to drive significant changes in grassland T_s.

Our analyses have shown that forests in the EUS exert a cooling effect on both surface and air temperatures, and that this effect can extend across ecosystem boundaries. Importantly, this cooling benefit is most pronounced during midday summer periods (Figures 3c and 3d; Figure 5b), which are typically associated with high heat stress and extreme events. These findings suggest that, in temperate zones, reforestation may provide the greatest climate adaptation benefit precisely when it is most needed.

4.2. Linking Reforestation to the Observed Lack of Warming in the Eastern US

To establish a link between reforestation and the observed lack of warming in the EUS, we analyzed historical weather station data to associate near-surface air temperature records with land cover changes during the 20th century. Additionally, we conducted a regional-scale analysis to investigate the relationship between spatial patterns of reforestation and temperature patterns in the EUS.

Overall, our analysis of long-term T_a records from 398 USHCN weather stations is consistent with the general understanding of 20th temperature trends in the EUS as it reveals no overall warming trend (Figures 1c and 5a). We observed a sharp decrease in average temperatures in the 1950s, which corresponds with previous studies that found an abrupt climactic regime shift in 1957–1958 in the EUS (Partridge et al., 2018; Rogers, 2013). The causes of this abrupt, uniform cooling are likely multifaceted. The abrupt cooling could be related to changes in jet stream position, specifically sharp decreases in the Meridional Circulation Index (MCI; Tosca et al., 2017). However, the impact of decreases in the MCI is greater on winter temperatures, which decreased more uniformly during the twentieth century than summer temperatures (Figure S11 in Supporting Information S1). Therefore, focusing on summer temperature time-series in addition to annual temperature time-series can help to distinguish the influence of the MCI from other mechanisms, including reforestation.

We investigated the signatures of reforestation in long-term climate data by analyzing the difference in long-term T_a records between weather stations predominantly surrounded by reforestation and nearby (within 50 km) weather stations that did not undergo land cover change (remained agriculture or forest) throughout the 20th century. In the early 20th century, we found that sites with nearby reforestation tended to be warmer than sites without reforestation in terms of maximum daily growing season temperatures (Figure 5b). This pattern is consistent with expectations if these areas were sparsely vegetated at the time (Figure 1), likely being abandoned agricultural or marginal lands with limited vegetation. As a result, these areas would have experienced lower rates of transpiration prior to reforestation, compared to their levels after reforestation. However, as the 20th century progressed, sites predominantly surrounded by reforestation became increasingly cool relative to their non-reforesting neighbors within 50 km. By the end of the 20th century, reforesting sites were up to 1°C cooler than their non-reforesting neighbors in terms of maximum growing season air temperatures (Figure 5b). The magnitude of the cooling effect is consistent with the results from the tower air temperature comparisons

(Figures 3c, 3d and 4), providing independent evidence of the impact of reforestation on near-surface air temperature.

Analysis of the forest cooling by age indicated that the cooling effect of regrowing forests takes about 20 years to fully develop, with forests around 20–40 years old exhibiting the strongest cooling effect (Figure 5c). This time frame is consistent with the time it takes for regenerating forests in the region to achieve levels of hydrological function comparable to mature forests (Ford et al., 2011). To offer historical context, during the growing season—when the cooling impact of regrowing forest is at its peak—reforesting sites were consistently cooler than nearby non-reforesting sites by the late 1950s (Figure 5b). This timeframe roughly corresponds to forests aged between 20 and 30 years, assuming the 1930s as a starting point due to widespread agricultural abandonment and federal reforestation efforts during that decade. The gap between maximum growing-season temperatures in forested versus nearby non-forested areas widened throughout the 20th century, supporting the idea that as forests grew, the summer cooling effect increased (Figure 5b).

Regional-scale analysis of gridded long-term air temperature data provided an independent, yet complementary approach to the weather station analyses. The analysis showed that younger forests were associated with lower historic rates of warming across most of the study region (Figure 5d). This finding, combined with the weather station analyses, suggests that reforestation had a cooling effect on near-surface air temperature across a wide swath of the EUS. Parsing the trends in long-term T_a time series as a function of land cover and historic land-cover change (e.g., the results in Figure 5) captures both the influence of regional-scale non-local effects and the finer-scale direct effects. However, we note studies focusing on 21st-century forest cover (e.g., Hansen et al., 2013) found considerable forest turnover in the EUS since 2000. If these findings accurately reflect forest dynamics, they could introduce complexities to the relationships presented in Figures 5d and 5c, which specifically explore the impact of forest age. Our methodology, employing aggregated data and spatial moving window analysis, is designed to mitigate the impact of these potential localized variations. Nonetheless, we recognize the potential for biases in our results related to forest age, particularly if the actual average stand age is systematically underestimated. We estimate that the potential impact of such a discrepancy on the conclusions drawn from our forest-age related findings is likely minimal. Even a considerable reduction in stand age (10 years) across a substantial portion (20%) of the study area would not alter the conclusions derived from Figures 5c and 5d (Figure S12 in Supporting Information S1).

While uncertainties remain regarding the characterization of forest age and historical land cover, our results support the expectation that 20th-century EUS reforestation had a net cooling effect that extended well beyond the surface and local stand-scale. For weather stations located near to, but outside of, reforested areas, the effect amounts to a suppression of T_a on the order of 0.5–1°C for the latter half of the 20th century.

4.3. Non-Local Effects of Land-Use Change

A more holistic perspective on the efficacy of nature-based climate solutions accounts for the possibility that local (e.g., ecosystem-scale) changes in land cover can initiate non-local impacts over much broader scales (Swann et al., 2012; Williams et al., 2021). For example, reforestation can lead to increased evapotranspiration, resulting in increased cloud cover and precipitation (Cerasoli et al., 2021; Manoli et al., 2016) that extend across the landscape. These effects would tend to amplify local cooling, particularly during the daytime. Localized land-cover changes can also cause shifts in atmospheric circulation, which can have continental or even global-scale consequences for temperature, precipitation, cloudiness, and other meteorological drivers (Pongratz et al., 2010; Swann et al., 2012; Winckler et al., 2019). Earth system models have been the primary tool for exploring these teleconnections, with many studies suggesting a dramatic role for non-local processes to amplify or counteract the local impacts of land-cover change on surface and near-surface temperature. However, results from these modeling studies are sometimes contradictory, and the difference between model predictions and observations can be large (Bonan, 2008; De Hertog et al., 2022). Notably, such discrepancies can include underestimations of the biophysical climate impacts associated with the expansion of vegetation cover (Li et al., 2020).

This study employs observational approaches to indirectly assess the non-local effects of land-cover change. We investigate how surface temperature effects can extend to the air and be transported across the landscape, providing a generalizable method to investigate these connections. Our approach includes exploring gradients in surface temperature (T_s) across ecosystem boundaries, as shown in Figure 4, to uncover the potential local extent

of such effects. This connection is crucial because long-term records of air temperature, which are used to delineate the warming hole, are made in open clearings. By uncovering how surface temperature effects extend to the air, we can gain insight into how local changes in land cover may initiate non-local impacts across much broader scales. It is important to note that these observational approaches have many limitations, as they cannot fully account for the possibility that non-local effects of land-use change within and outside the study region are influencing long-term temperature trends in the EUS.

For example, changes in agricultural management, such as agricultural intensification and increased irrigation use, are known to have a local cooling effect (Mueller et al., 2016), and many areas of the EUS have experienced these management shifts (Spangler et al., 2020). Changes in agricultural management that promote cooling could obscure the influence of reforestation in the comparison of long-term trends from forested and cropland ecosystems (e.g., Figure 5). Thus, the results presented here can be considered conservative. It is also possible that land-use changes occurring well outside of the study region may be driving widespread trends in long-term temperature trends in the EUS via teleconnections (Swann et al., 2018), or that certain non-local temperature effects of reforestation or deforestation may be opposite in sign to the local effects (De Hertog et al., 2022; Pongratz et al., 2021). These non-local teleconnections are currently only possible to explore with modeling studies that tend to rely on idealized experiments that force instantaneous and extreme changes in land cover across broad regions. Evaluating all modes of historical land-use change that might have affected climate in the EUS would be computationally expensive (if not impossible) and would still be unlikely to resolve, with precision, the relatively small changes in T_s and T_a that are revealed by the observation-driven approach taken here.

5. Conclusions

Various hypotheses have been proposed to explain the observed lack of 20th-century warming in the eastern United States (e.g., Meehl et al., 2012; Z. Pan et al., 2004; Partridge et al., 2018; Tosca et al., 2017). The work here does not identify widespread reforestation as the sole factor causing the EUS warming hole or its trend, but multiple independent data sources suggest it can be an important contributor to this lack of historic regional warming. Beyond that, the study provides robust evidence of local biophysical climate benefits of reforestation in the EUS. The strong and persistent increase in forest cover throughout the region in the 20th century contributed to cooling, which is consistent with observed temperature changes. In addition, the findings demonstrate that reforestation has a consistent cooling effect on both surface and air temperatures, especially during midsummer periods when high temperatures can be most harmful. These findings emphasize the potential for reforestation to provide local climate adaptation benefits in temperate regions such as the EUS, highlighting the importance of biophysical co-benefits of nature-based climate solutions.

Conflict of Interest

The authors declare no conflicts of interest relevant to this study.

Data Availability Statement

The AmeriFlux tower data utilized in this study are available from the AmeriFlux data portal (https://ameriflux.lbl.gov/). The various remote sensing and meteorological network data used are detailed in the methods section and can be accessed via the respective links and repositories mentioned therein. To ensure reproducibility and facilitate access to our research data, intermediate data products, code, and transformed data products (i.e., those derived from raw publicly available data) are publicly available in a Dryad repository (Barnes et al., 2024). The repository is maintained under a CC0 1.0 Universal (CC0 1.0) Public Domain Dedication license.

1. Daymet (Thornton et al., 2016) [Dataset]
   - Description: Daily surface weather data, including temperature, precipitation, and radiation.
   - Availability: The Daymet data on which this article is based are available in Thornton et al. (2016).
2. Ameriflux data
   - Description: Eddy covariance flux data and ancillary meteorological variables.
   - Availability: The Ameriflux sites used in this article are all available from the AmeriFlux data portal. https://ameriflux.lbl.gov/.
3. Eddy Covariance Data (Zhang et al., 2020)

- Description: Site descriptions and details on eddy covariance data processing for the six paired flux sites using the REddyProc processing tool (Wutzler et al., 2018).
- Availability: The data used in this study can be found in Zhang et al. (2020).

4. Temperature Extrapolation Model (Novick & Katul, 2020)
   - Description: Results for temperature extrapolation into the first 10 m of the surface layer after conceptual flattening of ecosystems.
   - Availability: Details and code for the temperature extrapolation model can be found in Novick and Katul (2020).
5. National Ecological Observatory Network (NEON) Towers (Metzger et al., 2019)
   - Description: Towers installed and operated by NEON for ecological observations.
   - Availability: Data from the NEON towers are available through Metzger et al. (2019). https://data.neonscience.org/data-products/DP4.00200.001.
6. AmeriFlux Biological, Ancillary Disturbance, and Metadata (BADM) Database
   - Description: Data from most towers available in the BADM database.
   - Availability: Data from the AmeriFlux towers can be accessed through the BADM database. https://ameriflux.lbl.gov/data/badm/.
7. Moderate Imaging Resolution Spectroradiometer (MODIS; Wan et al., 2015) [Dataset]
   - Description: MODIS data set for surface temperature (MYD11A1v6.1).
   - Availability: The MODIS data set used in this study is available in Wan et al. (2015).
8. U.S. Geological Survey North American Land-Cover Characteristics Data set (EROS, 2017) [Dataset]
   - Description: Land-cover characteristics data set.
   - Availability: The land-cover data set used in this study was provided by the U.S. Geological Survey's North American Land-Cover Characteristics project (EROS, 2017).
9. National Land Cover Database (NLCD) (Dewitz, 2019) [Dataset]
   - Description: Land cover data set used to identify forest-agriculture boundaries.
   - Availability: The National Land Cover Database (NLCD) data set used in this study can be accessed through Dewitz (2019).
10. Landsat Provisional Surface Temperature Product (Cook et al., 2014)
    - Description: Landsat-based surface temperature product.
    - Availability: The Landsat Provisional Surface Temperature Product used in this study is described in Cook et al. (2014) and can be accessed here: https://www.usgs.gov/landsat-missions/landsat-collection-1-us-analysis-ready-data.
11. FORE-SCE (Sohl, 2018)
    - Description: FOREcasting SCEnarios of Land-use Change backcasting grids from the US Land Cover Trends project.
    - Availability: The FORE-SCE grids used in this study are described in Sohl et al. (2007) and can be accessed through Sohl, 2018.
12. United States Historical Climate Network (USHCN) Meteorological Stations
    - Description: Meteorological station data for the United States.
    - Availability: Data from the USHCN meteorological stations are available through the respective network. https://www.ncei.noaa.gov/products/land-based-station/us-historical-climatology-network.
13. University of Delaware Air Temperature and Precipitation Data set (Willmott & Matsuura, 2015) [Dataset]
    - Description: Monthly temperature timeseries with a spatial resolution of 0.5°.
    - Availability: The University of Delaware Air Temperature and Precipitation Data set used in this study is provided by Willmott and Matsuura (2015) through NOAA/OAR/ESRL PSD.
14. "greenbrown" R Package (Forkel & Wutzler, 2015) [Software]
    - Description: R package used for season-trend model estimation.
    - Availability: The "greenbrown" R package can be accessed through Forkel and Wutzler (2015).
15. North American Carbon Program (NACP) Forest Age Maps (Y. Pan et al., 2012) [Dataset]
    - Description: Forest age maps for the year 2006.
    - Availability: The North American Carbon Program (NACP) forest age maps are available through Y. Pan et al. (2012).
16. "SpatialEco" R Package (Evans, 2021) [Software]
    - Description: R package for spatial ecological analysis.

- Availability: The "SpatialEco" R package used in this study is provided by Evans (2021).

17. "raster" R Package (Hijmans, 2021) [Software].
    - Description: R package with the "modal" function used in the analysis.
    - Availability: The "raster" R package with function is available through Hijmans (2021).

Acknowledgments

The authors acknowledge Mike Voyles, Michael Benson, Steve Scott, Koong Yi, Matt Wenzel, and Chris Sobek for their help in installing and maintaining the paired flux tower sites. The findings and conclusions in this publication are those of the authors and should not be construed to represent any official USDA or US Government determination or policy. The authors declare no competing interests. Funding was provided by the US National Science Foundation (NSF) grant through Grants NSF-DEB-1552747, NSF-DEB-1637522, NSF-IOS-1754893, and NSF-AGS-2028633. KAN and ACO also acknowledge support from the USDA Forest Service—Southern Research Station. GK acknowledges support from the US Department of Energy (DOE) Office of Science (DE-SC0022072). QZ acknowledges support from the National Natural Science Foundation of China (U2243214). Funding for the AmeriFlux data portal was provided by the DOE Office of Science. This material is based in part on work supported by the NSF through the National Ecological Observatory Network (NEON) program. The authors thank the AmeriFlux tower PIs for generously sharing their data.

References

Anderegg, W. R. L., Chegwidden, O. S., Badgley, G., Trugman, A. T., Cullenward, D., Abatzoglou, J. T., et al. (2022). Future climate risks from stress, insects and fire across US forests. *Ecology Letters*, *25*(6), 1510–1520. https://doi.org/10.1111/ele.14018

Anderson, R. G., Canadell, J. G., Randerson, J. T., Jackson, R. B., Hungate, B. A., Baldocchi, D. D., et al. (2011). Biophysical considerations in forestry for climate protection. *Frontiers in Ecology and the Environment*, *9*(3), 174–182. https://doi.org/10.1890/090179

Baldocchi, D., & Ma, S. (2013). How will land use affect air temperature in the surface boundary layer? Lessons learned from a comparative study on the energy balance of an oak savanna and annual grassland in California, USA. *Tellus B: Chemical and Physical Meteorology*, *65*(1), 19994. https://doi.org/10.3402/tellusb.v65i0.19994

Barbero, R., Abatzoglou, J. T., Larkin, N. K., Kolden, C. A., & Stocks, B. (2015). Climate change presents increased potential for very large fires in the contiguous United States. *International Journal of Wildland Fire*, *24*(7), 892. https://doi.org/10.1071/WF15083

Barnes, M., Zhang, Q., Robeson, S., Young, L., Burakowski, E., Oishi, A. C., et al. (2024). Data and code for: A century of reforestation reduced anthropogenic warming in the eastern United States [Dataset]. Dryad. https://doi.org/10.5061/dryad.w0vt4b8wk

Bentz, B. J., Régnière, J., Fettig, C. J., Hansen, E. M., Hayes, J. L., Hicke, J. A., et al. (2010). Climate change and bark beetles of the Western United States and Canada: Direct and indirect effects. *BioScience*, *60*(8), 602–613. https://doi.org/10.1525/bio.2010.60.8.6

Bonan, G. B. (2001). Observational evidence for reduction of daily maximum temperature by Croplands in the midwest United States. *Journal of Climate*, *14*(11), 2430–2442. https://doi.org/10.1175/1520-0442(2001)014<2430:OEFROD>2.0.CO;2

Bonan, G. B. (2008). Forests and climate change: Forcings, feedbacks, and the climate benefits of forests. *Science*, *320*(5882), 1444–1449. https://doi.org/10.1126/science.1155121

Bright, R. M., Davin, E., O'Halloran, T., Pongratz, J., Zhao, K., & Cescatti, A. (2017). Local temperature response to land cover and management change driven by non-radiative processes. *Nature Climate Change*, *7*(4), 296–302. https://doi.org/10.1038/nclimate3250

Burakowski, E., Tawfik, A., Ouimette, A., Lepine, L., Novick, K., Ollinger, S., et al. (2018). The role of surface roughness, albedo, and Bowen ratio on ecosystem energy balance in the Eastern United States. *Agricultural and Forest Meteorology*, *249*, 367–376. https://doi.org/10.1016/j.agrformet.2017.11.030

Carman, S. F. (2013). Indiana forest management history and practices Tech. Rep. NRS-P-108. In R. K. Swihart, M. R. Saunders, R. A. Kalb, G. S. Haulton, & C. H. Michler (Eds.), *The hardwood ecosystem experiment: A framework for studying responses to forest management* (pp. 12–23). USDA Forest Service Gen. Retrieved from https://www.nrs.fs.fed.us/pubs/42897

Cerasoli, S., Yin, J., & Porporato, A. (2021). Cloud cooling effects of afforestation and reforestation at midlatitudes. *Proceedings of the National Academy of Sciences of the United States of America*, *118*(33), e2026241118. https://doi.org/10.1073/pnas.2026241118

Cohn, A. S., Bhattarai, N., Campolo, J., Crompton, O., Dralle, D., Duncan, J., & Thompson, S. (2019). Forest loss in Brazil increases maximum temperatures within 50 km. *Environmental Research Letters*, *14*(8), 084047. https://doi.org/10.1088/1748-9326/ab31fb

Cook, M. (2014). *Atmospheric compensation for a Landsat land surface temperature product*. Theses. Retrieved from https://scholarworks.rit.edu/theses/8513

Cook, M., Schott, J. R., Mandel, J., & Raqueno, N. (2014). Development of an operational calibration methodology for the Landsat thermal data archive and initial testing of the atmospheric compensation component of a land surface temperature (LST) product from the archive. *Remote Sensing*, *6*(11), 11244–11266. https://doi.org/10.3390/rs61111244

De Hertog, S. J., Havermann, F., Vanderkelen, I., Guo, S., Luo, F., Manola, I., et al. (2022). The biogeophysical effects of idealized land cover and land management changes in Earth system models. *Earth System Dynamics*, *13*(3), 1305–1350. https://doi.org/10.5194/esd-13-1305-2022

Dewitz, J. (2019). National land cover dataset (NLCD) 2016 products [Dataset]. U.S. Geological Survey. https://doi.org/10.5066/P96HHBIE

Earth Resources Observation And Science (EROS) Center. (2017). Global land cover characterization (GLCC) [Dataset]. U.S. Geological Survey. https://doi.org/10.5066/F7GB230D

Evans, J. S. (2021). spatialEco. R package version 1.3-6 [Software]. Retrieved from https://github.com/jeffreyevans/spatialEco

Farella, M. M., Fisher, J. B., Jiao, W., Key, K. B., & Barnes, M. L. (2022). Thermal remote sensing for plant ecology from leaf to globe. *Journal of Ecology*, *110*(9), 1996–2014. https://doi.org/10.1111/1365-2745.13957

Ford, C. R., Laseter, S. H., Swank, W. T., & Vose, J. M. (2011). Can forest management be used to sustain water-based ecosystem services in the face of climate change? *Ecological Applications*, *21*(6), 2049–2067. https://doi.org/10.1890/10-2246.1

Forkel, M., & Wutzler, T. (2015). Greenbrown—Land surface phenology and trend analysis. A package for the R software. (Version 2.2) [Software]. Retrieved from http://greenbrown.r-forge.r-project.org/

Griscom, B. W., Adams, J., Ellis, P. W., Houghton, R. A., Lomax, G., Miteva, D. A., et al. (2017). Natural climate solutions. *Proceedings of the National Academy of Sciences of the United States of America*, *114*(44), 11645–11650. https://doi.org/10.1073/pnas.1710465114

Hall, B., Motzkin, G., Foster, D. R., Syfert, M., & Burk, J. (2002). Three hundred years of forest and land-use change in Massachusetts, USA. *Journal of Biogeography*, *29*(10–11), 1319–1335. https://doi.org/10.1046/j.1365-2699.2002.00790.x

Hansen, M. C., Potapov, P. V., Moore, R., Hancher, M., Turubanova, S. A., Tyukavina, A., et al. (2013). High-resolution global maps of 21st-century forest cover change. *Science*, *342*(6160), 850–853. https://doi.org/10.1126/science.1244693

Helbig, M., Gerken, T., Beamesderfer, E. R., Baldocchi, D. D., Banerjee, T., Biraud, S. C., et al. (2021). Integrating continuous atmospheric boundary layer and tower-based flux measurements to advance understanding of land-atmosphere interactions. *Agricultural and Forest Meteorology*, *307*, 108509. https://doi.org/10.1016/j.agrformet.2021.108509

Hijmans, R. (2021). raster: Geographic data analysis and modeling [Software]. R package version 3.5-9. Retrieved from https://CRAN.R-project.org/package=raster

Houghton, R. A., & Hackler, J. L. (2000). Changes in terrestrial carbon storage in the United States. 1: The roles of agriculture and forestry. *Global Ecology and Biogeography*, *9*(2), 125–144. https://doi.org/10.1046/j.1365-2699.2000.00166.x

Hsieh, C.-I., & Katul, G. (2009). The Lagrangian stochastic model for estimating footprint and water vapor fluxes over inhomogeneous surfaces. *International Journal of Biometeorology*, *53*(1), 87–100. https://doi.org/10.1007/s00484-008-0193-0

Juang, J.-Y., Katul, G., Siqueira, M., Stoy, P., & Novick, K. (2007). Separating the effects of albedo from eco-physiological changes on surface temperature along a successional chronosequence in the southeastern United States. *Geophysical Research Letters*, *34*(21), L21408. https://doi.org/10.1029/2007GL031296

Lee, X., Goulden, M. L., Hollinger, D. Y., Barr, A., Black, T. A., Bohrer, G., et al. (2011). Observed increase in local cooling effect of deforestation at higher latitudes. *Nature*, *479*(7373), 384–387. https://doi.org/10.1038/nature10588
Li, D., & Wang, L. (2019). Sensitivity of surface temperature to land use and land cover change-induced biophysical changes: The scale issue. *Geophysical Research Letters*, *46*(16), 9678–9689. https://doi.org/10.1029/2019GL084861
Li, Y., Piao, S., Chen, A., Ciais, P., & Li, L. Z. X. (2020). Local and teleconnected temperature effects of afforestation and vegetation greening in China. *National Science Review*, *7*(5), 897–912. https://doi.org/10.1093/nsr/nwz132
Liu, Z., Ballantyne, A. P., & Cooper, L. A. (2019). Biophysical feedback of global forest fires on surface temperature. *Nature Communications*, *10*(1), 214. https://doi.org/10.1038/s41467-018-08237-z
Loveland, T. R., Zhu, Z., Ohlen, D. O., Brown, J. F., Reed, B. C., & Yang, L. (1999). An analysis of the IGBP global land-cover characterization process. *An Analysis of the IGBP Global Land-Cover Characterization Process*, *65*(9), 1021–1032.
Mahmood, R., Pielke, R. A., Sr., Hubbard, K. G., Niyogi, D., Dirmeyer, P. A., McAlpine, C., et al. (2014). Land cover changes and their biogeophysical effects on climate. *International Journal of Climatology*, *34*(4), 929–953. https://doi.org/10.1002/joc.3736
Manoli, G., Domec, J., Novick, K., Oishi, A. C., Noormets, A., Marani, M., & Katul, G. (2016). Soil–plant–atmosphere conditions regulating convective cloud formation above southeastern US pine plantations. *Global Change Biology*, *22*(6), 2238–2254. https://doi.org/10.1111/gcb.13221
Mascioli, N. R., Previdi, M., Fiore, A. M., & Ting, M. (2017). Timing and seasonality of the United States' warming hole. *Environmental Research Letters*, *12*(3), 034008. https://doi.org/10.1088/1748-9326/aa5ef4
Meehl, G. A., Arblaster, J. M., & Branstator, G. (2012). Mechanisms contributing to the warming hole and the consequent U.S. East–West differential of heat extremes. *Journal of Climate*, *25*(18), 6394–6408. https://doi.org/10.1175/JCLI-D-11-00655.1
Metzger, S., Ayres, E., Durden, D., Florian, C., Lee, R., Lunch, C., et al. (2019). From NEON field sites to data portal: A community resource for surface–atmosphere research comes online. *Bulletin of the American Meteorological Society*, *100*(11), 2305–2325. https://doi.org/10.1175/BAMS-D-17-0307.1
Mildrexler, D. J., Zhao, M., & Running, S. W. (2011). A global comparison between station air temperatures and MODIS land surface temperatures reveals the cooling role of forests. *Journal of Geophysical Research*, *116*(G3), G03025. https://doi.org/10.1029/2010jg001486
Monin, A. S., & Obukhov, A. M. (1954). Basic laws of turbulent mixing in the surface layer of the atmosphere. *Trudy – Geologicheskiy Institut, Akademiya Nauk SSSR*, *24*, 163–187.
Mueller, N. D., Butler, E. E., McKinnon, K. A., Rhines, A., Tingley, M., Holbrook, N. M., & Huybers, P. (2016). Cooling of US Midwest summer temperature extremes from cropland intensification. *Nature Climate Change*, *6*(3), 317–322. https://doi.org/10.1038/nclimate2825
Nolan, C. J., Field, C. B., & Mach, K. J. (2021). Constraints and enablers for increasing carbon storage in the terrestrial biosphere. *Nature Reviews Earth and Environment*, *2*(6), 436–446. https://doi.org/10.1038/s43017-021-00166-8
Novick, K., Biederman, J. A., Desai, A. R., Litvak, M. E., Moore, D. J., Scott, R. L., & Torn, M. S. (2018). The AmeriFlux network: A coalition of the willing. *Agricultural and Forest Meteorology*, *249*, 444–456. https://doi.org/10.1016/j.agrformet.2017.10.009
Novick, K., Jo, I., D'Orangeville, L., Benson, M., Au, T. F., Barnes, M., et al. (2022). The drought response of eastern US Oaks in the context of their declining abundance. *BioScience*, *72*(4), 333–346. https://doi.org/10.1093/biosci/biab135
Novick, K., & Katul, G. G. (2020). The duality of reforestation impacts on surface and air temperature. *Journal of Geophysical Research: Biogeosciences*, *125*(4). https://doi.org/10.1029/2019JG005543
Novick, K., Metzger, S., Anderegg, W. R. L., Barnes, M., Cala, D. S., Guan, K., et al. (2022). Informing Nature-based Climate Solutions for the United States with the best-available science. *Global Change Biology*, *28*(12), 3778–3794. https://doi.org/10.1111/gcb.16156
Novick, K. A., & Barnes, M. L. (2023). A practical exploration of land cover impacts on surface and air temperature when they are most consequential. *Environmental Research: Climate*, *2*(2), 025007. https://doi.org/10.1088/2752-5295/accdf9
Novick, K. A., Williams, C., Rankle, B., Anderegg, W., Hollinger, D., Litvak, M., et al. (2022). The science needed for robust, scalable, and credible nature-based climate solutions in the United States: Full Report. IUScholarWorks. https://doi.org/10.5967/N7R9-7J83
Nowacki, G. J., & Abrams, M. D. (2008). The demise of fire and "Mesophication" of forests in the eastern United States. *BioScience*, *58*(2), 123–138. https://doi.org/10.1641/B580207
Pan, Y., Chen, J. M., Birdsey, R., McCullough, K., He, L., & Deng, F. (2012). NACP Forest Age Maps at 1-km Resolution for Canada (2004) and the U.S.A. (2006) [Dataset]. https://doi.org/10.3334/ORNLDAAC/1096
Pan, Z., Arritt, R. W., Takle, E. S., Gutowski, W. J., Anderson, C. J., & Segal, M. (2004). Altered hydrologic feedback in a warming climate introduces a "warming hole". *Geophysical Research Letters*, *31*(17). https://doi.org/10.1029/2004GL020528
Partridge, T. F., Winter, J. M., Osterberg, E. C., Hyndman, D. W., Kendall, A. D., & Magilligan, F. J. (2018). Spatially distinct seasonal patterns and forcings of the U.S. Warming Hole. *Geophysical Research Letters*, *45*(4), 2055–2063. https://doi.org/10.1002/2017GL076463
Peng, S.-S., Piao, S., Zeng, Z., Ciais, P., Zhou, L., Li, L. Z. X., et al. (2014). Afforestation in China cools local land surface temperature. *Proceedings of the National Academy of Sciences of the United States of America*, *111*(8), 2915–2919. https://doi.org/10.1073/pnas.1315126111
Pongratz, J., Reick, C. H., Raddatz, T., & Claussen, M. (2010). Biogeophysical versus biogeochemical climate response to historical anthropogenic land cover change: Climate effects of historical land cover change. *Geophysical Research Letters*, *37*(8). https://doi.org/10.1029/2010GL043010
Pongratz, J., Schwingshackl, C., Bultan, S., Obermeier, W., Havermann, F., & Guo, S. (2021). Land Use Effects on Climate: Current State, Recent Progress, and Emerging Topics. *Current Climate Change Reports*, *7*(4), 99–120. https://doi.org/10.1007/s40641-021-00178-y
Ramankutty, N., Heller, E., & Rhemtulla, J. (2010). Prevailing myths about agricultural abandonment and forest regrowth in the United States. *Annals of the Association of American Geographers*, *100*(3), 502–512. https://doi.org/10.1080/00045601003788876
Randerson, J. T., Liu, H., Flanner, M. G., Chambers, S. D., Jin, Y., Hess, P. G., et al. (2006). The impact of boreal forest fire on climate warming. *Science*, *314*(5802), 1130–1132. https://doi.org/10.1126/science.1132075
R Core Team. (2020). R: A language and environment for statistical computing [Software]. R Foundation for Statistical Computing. Retrieved from https://www.R-project.org/
Rogers, J. C. (2013). The 20th century cooling trend over the southeastern United States. *Climate Dynamics*, *40*(1), 341–352. https://doi.org/10.1007/s00382-012-1437-6
Seddon, N., Chausson, A., Berry, P., Girardin, C. A. J., Smith, A., & Turner, B. (2020). Understanding the value and limits of nature-based solutions to climate change and other global challenges. *Philosophical Transactions of the Royal Society B: Biological Sciences*, *375*(1794), 20190120. https://doi.org/10.1098/rstb.2019.0120
Sohl, T. L. (2018). Modeled Historical Land Use and Land Cover for the Conterminous United States: 1938-1992 [Dataset]. U.S. Geological Survey. https://doi.org/10.5066/F7KK99RR
Sohl, T. L., Sayler, K. L., Drummond, M. A., & Loveland, T. R. (2007). The FORE-SCE model: A practical approach for projecting land cover change using scenario-based modeling. *Journal of Land Use Science*, *2*(2), 103–126. https://doi.org/10.1080/17474230701218202
Spangler, K., Burchfield, E. K., & Schumacher, B. (2020). Past and current dynamics of U.S. agricultural land use and policy. *Frontiers in Sustainable Food Systems*, *4*, 98. https://doi.org/10.3389/fsufs.2020.00098

Swann, A. L., Fung, I. Y., Levis, S., Bonan, G. B., & Doney, S. C. (2010). Changes in Arctic vegetation amplify high-latitude warming through the greenhouse effect. *Proceedings of the National Academy of Sciences of the United States of America*, *107*(4), 1295–1300. https://doi.org/10.1073/pnas.0913846107

Swann, A. L. S., Fung, I. Y., & Chiang, J. C. H. (2012). Mid-latitude afforestation shifts general circulation and tropical precipitation. *Proceedings of the National Academy of Sciences of the United States of America*, *109*(3), 712–716. https://doi.org/10.1073/pnas.1116706108

Swann, A. L. S., Laguë, M. M., Garcia, E. S., Field, J. P., Breshears, D. D., Moore, D. J. P., et al. (2018). Continental-scale consequences of tree die-offs in North America: Identifying where forest loss matters most. *Environmental Research Letters*, *13*(5), 055014. https://doi.org/10.1088/1748-9326/aaba0f

Thornton, P. E., Thornton, M. M., Mayer, B. W., Wei, Y., Devarakonda, R., Vose, R. S., & Cook, R. B. (2016). Daymet: Daily surface weather data on a 1-km grid for North America, version 3 (Version 3.4) [Dataset]. 0 MB. https://doi.org/10.3334/ORNLDAAC/1328

Tosca, M. G., Campbell, J., Garay, M., Lolli, S., Seidel, F. C., Marquis, J., & Kalashnikova, O. (2017). Attributing accelerated summertime warming in the Southeast United States to recent reductions in aerosol burden: Indications from vertically-resolved observations. *Remote Sensing*, *9*(7), 674. https://doi.org/10.3390/rs9070674

Tyukavina, A., Potapov, P., Hansen, M. C., Pickens, A. H., Stehman, S. V., Turubanova, S., et al. (2022). Global trends of forest loss due to fire from 2001 to 2019. *Frontiers in Remote Sensing*, *3*, 825190. https://doi.org/10.3389/frsen.2022.825190

Van Wees, D., Van Der Werf, G. R., Randerson, J. T., Andela, N., Chen, Y., & Morton, D. C. (2021). The role of fire in global forest loss dynamics. *Global Change Biology*, *27*(11), 2377–2391. https://doi.org/10.1111/gcb.15591

Verbesselt, J., Hyndman, R., Zeileis, A., & Culvenor, D. (2010). Phenological change detection while accounting for abrupt and gradual trends in satellite image time series. *Remote Sensing of Environment*, *114*(12), 2970–2980. https://doi.org/10.1016/j.rse.2010.08.003

Verbesselt, J., Zeileis, A., & Herold, M. (2012). Near real-time disturbance detection using satellite image time series. *Remote Sensing of Environment*, *123*, 98–108. https://doi.org/10.1016/j.rse.2012.02.022

Wan, Z., Hook, S., & Hulley, G. (2015). MYD11A1 MODIS/Aqua Land Surface Temperature/Emissivity Daily L3 Global 1km SIN Grid V006 [Dataset]. NASA EOSDIS Land Processes DAAC. https://doi.org/10.5067/MODIS/MYD11A1.006

Wear, D. N., & Greis, J. G. (2012). *The southern forest futures project: Summary report*. Gen. Tech. Rep. SRS-GTR-168 (Vol. 168, pp. 1–54). USDA-Forest Service, Southern Research Station.

Williams, C. A., Gu, H., & Jiao, T. (2021). Climate impacts of U.S. forest loss span net warming to net cooling. *Science Advances*, *7*(7), eaax8859. https://doi.org/10.1126/sciadv.aax8859

Willmott, C. J., & Matsuura, K. (2015). Terrestrial Air Temperature and Precipitation: Monthly and Annual Time Series (V4.01; 1900-2014) [Dataset]. Retrieved from http://climate.geog.udel.edu/climate/html_pages/README.ghcn_ts2.html

Willmott, C. J., & Matsuura, K. (1995). Smart Interpolation of Annually Averaged Air Temperature in the United States. *Journal of Applied Meteorology*, *34*(12), 2577–2586. https://doi.org/10.1175/1520-0450(1995)034<2577:SIOAAA>2.0.CO;2

Winckler, J., Reick, C. H., Luyssaert, S., Cescatti, A., Stoy, P. C., Lejeune, Q., et al. (2019). Different response of surface temperature and air temperature to deforestation in climate models. *Earth System Dynamics*, *10*(3), 473–484. https://doi.org/10.5194/esd-10-473-2019

Windisch, M. G., Davin, E. L., & Seneviratne, S. I. (2021). Prioritizing forestation based on biogeochemical and local biogeophysical impacts. *Nature Climate Change*, *11*(10), 867–871. https://doi.org/10.1038/s41558-021-01161-z

Wutzler, T., Lucas-Moffat, A., Migliavacca, M., Knauer, J., Sickel, K., Šigut, L., et al. (2018). Basic and extensible post-processing of eddy covariance flux data with REddyProc. *Biogeosciences*, *15*(16), 5015–5030. https://doi.org/10.5194/bg-15-5015-2018

Zhang, Q., Barnes, M., Benson, M., Burakowski, E., Oishi, A. C., Ouimette, A., et al. (2020). Reforestation and surface cooling in temperate zones: Mechanisms and implications. *Global Change Biology*, *26*(6), 3384–3401. https://doi.org/10.1111/gcb.15069

References From the Supporting Information

Baker, J., & Griffis, T. (2016). AmeriFlux BASE US-Ro1 Rosemount- G21, Ver. 5-5 [Dataset]. AmeriFlux AMP. https://doi.org/10.17190/AMF/1246092

Baker, J., & Griffis, T. (2021). AmeriFlux FLUXNET-1F US-Ro5 Rosemount I18_South, Ver. 3-5 [Dataset]. AmeriFlux AMP. https://doi.org/10.17190/AMF/1818371

Baker, J., & Griffis, T. (2018). AmeriFlux BASE US-Ro6 Rosemount I18_North, Ver. 14-5 [Dataset]. AmeriFlux AMP. https://doi.org/10.17190/AMF/1419509

Bernacchi, C. (2016). AmeriFlux BASE US-Bo2 Bondville (companion site), Ver. 2-1 [Dataset]. AmeriFlux AMP. https://doi.org/10.17190/AMF/1246037

Billesbach, D., Kueppers, L., Torn, M., & Biraud, S. (2018a). AmeriFlux BASE US-A32 ARM-SGP Medford hay pasture, Ver. 1-5 [Dataset]. AmeriFlux AMP. https://doi.org/10.17190/AMF/1436327

Billesbach, D., Kueppers, L., Torn, M., & Biraud, S. (2018b). AmeriFlux BASE US-A74 ARM SGP milo field, Ver. 1-5 [Dataset]. AmeriFlux AMP. https://doi.org/10.17190/AMF/1436328

Billesbach, D., Bradford, J., & Torn, M. (2019a). AmeriFlux BASE US-AR1 ARM USDA UNL OSU Woodward Switchgrass 1, Ver. 3-5 [Dataset]. AmeriFlux AMP. https://doi.org/10.17190/AMF/1246137

Billesbach, D., Bradford, J., & Torn, M. (2019b). AmeriFlux BASE US-AR2 ARM USDA UNL OSU Woodward Switchgrass 2, Ver. 3-5 [Dataset]. AmeriFlux AMP. https://doi.org/10.17190/AMF/1246138

Biraud, S., Fischer, M., Chan, S., & Torn, M. (2021). AmeriFlux BASE US-ARM ARM Southern Great Plains site- Lamont, Ver. 11-5 [Dataset]. AmeriFlux AMP. https://doi.org/10.17190/AMF/1246027

Brunsell, N. (2020a). AmeriFlux BASE US-KFS Kansas Field Station, Ver. 7-5 [Dataset]. AmeriFlux AMP. https://doi.org/10.17190/AMF/1246132

Brunsell, N. (2020b). AmeriFlux BASE US-Kon Konza Prairie LTER (KNZ), Ver. 5-5 [Dataset]. AmeriFlux AMP. https://doi.org/10.17190/AMF/1246068

Chen, J., & Chu, H. (2021). AmeriFlux BASE US-CRT Curtice Walter-Berger cropland, Ver. 5-5 [Dataset]. AmeriFlux AMP. https://doi.org/10.17190/AMF/1246156

Chen, J., Chu, H., & Noormets, A. (2008). AmeriFlux BASE US-Oho Oak Openings, Ver. 7-5 [Dataset]. AmeriFlux AMP. https://doi.org/10.17190/AMF/1246089

Clark, K. (2016). AmeriFlux BASE US-Slt Silas Little- New Jersey, Ver. 5-1 [Dataset]. AmeriFlux AMP. https://doi.org/10.17190/AMF/1246096

Duff, A., & Desai, A. (2020). AmeriFlux BASE US-DFC US Dairy Forage Research Center, Prairie du Sac, Ver. 1-5 [Dataset]. AmeriFlux AMP. https://doi.org/10.17190/AMF/1660340

Goslee, S. (2021). AmeriFlux BASE US-HWB USDA ARS Pasture Sytems and Watershed Management Research Unit- Hawbecker Site, Ver. 1-5 [Dataset]. AmeriFlux AMP. https://doi.org/10.17190/AMF/1811363
Hollinger, D. (2021). AmeriFlux BASE US-Ho1 Howland Forest (main tower), Ver. 7-5 [Dataset]. AmeriFlux AMP. https://doi.org/10.17190/AMF/1246061
Kelsey, E., & Green, M. (2020). AmeriFlux BASE US-HBK Hubbard Brook Experimental Forest, Ver. 1-5 [Dataset]. AmeriFlux AMP. https://doi.org/10.17190/AMF/1634881
Melillo, J. M., Richmond, T. T. C., & Yohe, G. W. (2014). *Climate change impacts in the United States: The third National climate assessment*. U. S. Global Change Research Program. https://doi.org/10.7930/J0Z31WJ2
Meyers, T. (2016). AmeriFlux BASE US-Bo1 Bondville, Ver. 2-1 [Dataset]. AmeriFlux AMP. https://doi.org/10.17190/AMF/1246036
McFadden, J. (2016). AmeriFlux BASE US-KUT KUOM Turfgrass Field, Ver. 1-1 [Dataset]. AmeriFlux AMP. https://doi.org/10.17190/AMF/1246145
NEON (National Ecological Observatory Network). (2021a). AmeriFlux BASE US-xAE NEON Klemme Range Research Station (OAES), Ver. 3-5 [Dataset]. AmeriFlux AMP. https://doi.org/10.17190/AMF/1671891
NEON (National Ecological Observatory Network). (2021b). AmeriFlux BASE US-xBL NEON Blandy Experimental Farm (BLAN), Ver. 3-5 [Dataset]. AmeriFlux AMP. https://doi.org/10.17190/AMF/1671893
NEON (National Ecological Observatory Network). (2021c). AmeriFlux BASE US-xCL NEON LBJ National Grassland (CLBJ), Ver. 3-5 [Dataset]. AmeriFlux AMP. https://doi.org/10.17190/AMF/1671894
NEON (National Ecological Observatory Network). (2021d). AmeriFlux BASE US-xDL NEON Dead Lake (DELA), Ver. 4-5 [Dataset]. AmeriFlux AMP. https://doi.org/10.17190/AMF/1579721
NEON (National Ecological Observatory Network). (2021e). AmeriFlux BASE US-xKA NEON Konza Prairie Biological Station - Relocatable (KONA), Ver. 4-5 [Dataset]. AmeriFlux AMP. https://doi.org/10.17190/AMF/1579722
NEON (National Ecological Observatory Network). (2021f). AmeriFlux BASE US-xKZ NEON Konza Prairie Biological Station (KONZ), Ver. 5-5 [Dataset]. AmeriFlux AMP. https://doi.org/10.17190/AMF/1562392
NEON (National Ecological Observatory Network). (2021g). AmeriFlux BASE US-xLE NEON Lenoir Landing (LENO), Ver. 2-5 [Dataset]. AmeriFlux AMP. https://doi.org/10.17190/AMF/1773398
NEON (National Ecological Observatory Network). (2021h). AmeriFlux BASE US-xSB NEON Ordway-Swisher Biological Station (OSBS), Ver. 3-5 [Dataset]. AmeriFlux AMP. https://doi.org/10.17190/AMF/1671899
NEON (National Ecological Observatory Network). (2021i). AmeriFlux BASE US-xSC NEON Smithsonian Conservation Biology Institute (SCBI), Ver. 3-5 [Dataset]. AmeriFlux AMP. https://doi.org/10.17190/AMF/1671900
NEON (National Ecological Observatory Network). (2021j). AmeriFlux BASE US-xSE NEON Smithsonian Environmental Research Center (SERC), Ver. 4-5 [Dataset]. AmeriFlux AMP. https://doi.org/10.17190/AMF/1617734
NEON (National Ecological Observatory Network). (2021k). AmeriFlux BASE US-xST NEON Steigerwaldt Land Services (STEI), Ver. 4-5 [Dataset]. AmeriFlux AMP. https://doi.org/10.17190/AMF/1617737
NEON (National Ecological Observatory Network). (2021l). AmeriFlux BASE US-xTA NEON Talladega National Forest (TALL), Ver. 3-5 [Dataset]. AmeriFlux AMP. https://doi.org/10.17190/AMF/1671902
NEON (National Ecological Observatory Network). (2021m). AmeriFlux BASE US-xTR NEON Treehaven (TREE), Ver. 4-5 [Dataset]. AmeriFlux AMP. https://doi.org/10.17190/AMF/1634886
Noormets, A. (2018a). AmeriFlux BASE US-NC1 NC_Clearcut, Ver. 3-5 [Dataset]. AmeriFlux AMP. https://doi.org/10.17190/AMF/1246082
Noormets, A. (2018b). AmeriFlux BASE US-NC3 NC_Clearcut#3, Ver. 3-5 [Dataset]. AmeriFlux AMP. https://doi.org/10.17190/AMF/1419506
Noormets, A., Mitra, B., Sun, G., Miao, G., King, J., Minick, K., et al. (2021). AmeriFlux BASE US-C2 NC_Loblolly Plantation, Ver. 9-5 [Dataset]. AmeriFlux AMP. https://doi.org/10.17190/AMF/1246083
Novick, K., & Phillips, R. (2021). AmeriFlux BASE US-MMS Morgan Monroe State Forest, Ver. 20-5 [Dataset]. AmeriFlux AMP. https://doi.org/10.17190/AMF/1246080
Novick, K. (2020). AmeriFlux BASE US-BRG Bayles Road Grassland Tower, Ver. 1-5 [Dataset]. AmeriFlux AMP. https://doi.org/10.17190/AMF/1756416
Oishi, A. C. (2020). AmeriFlux BASE US-Cwt Coweeta, Ver. 1-5 [Dataset]. AmeriFlux AMP. https://doi.org/10.17190/AMF/1671890
Oishi, A. C., Novick, K., & Stoy, P. (2018a). AmeriFlux BASE US-Dk1 Duke Forest-open field, Ver. 4-5 [Dataset]. AmeriFlux AMP. https://doi.org/10.17190/AMF/1246046
Oishi, A. C., Novick, K., & Stoy, P. (2018b). AmeriFlux BASE US-Dk2 Duke Forest-hardwoods, Ver. 4-5 [Dataset]. AmeriFlux AMP. https://doi.org/10.17190/AMF/1246047
Oishi, A. C., Novick, K., & Stoy, P. (2018c). AmeriFlux BASE US-Dk3 Duke Forest - Loblolly pine, Ver. 4-5 [Dataset]. AmeriFlux AMP. https://doi.org/10.17190/AMF/1246048
Robertson, G. P., & Chen, J. (2021). AmeriFlux BASE US-KM4 KBS Marshall Farms Smooth Brome Grass (Ref), Ver. 4-5 [Dataset]. AmeriFlux AMP. https://doi.org/10.17190/AMF/1634882
Starr, G. (2021a). AmeriFlux BASE US-LL1 Longleaf Pine - Baker (Mesic site), Ver. 2-5 [Dataset]. AmeriFlux AMP. https://doi.org/10.17190/AMF/1773395
Starr, G. (2021b). AmeriFlux BASE US-LL2 Longleaf Pine - Dubignion (Intermediate site), Ver. 1-5 [Dataset]. AmeriFlux AMP. https://doi.org/10.17190/AMF/1773396
Starr, G. (2021c). AmeriFlux BASE US-LL3 Longleaf Pine - Red Dirt (Xeric site), Ver. 1-5 [Dataset]. AmeriFlux AMP. https://doi.org/10.17190/AMF/1773397
Suyker, A. (2016a). AmeriFlux BASE US-Ne1 Mead - Irrigated continuous maize site, Ver. 11-5 [Dataset]. AmeriFlux AMP. https://doi.org/10.17190/AMF/1246084
Suyker, A. (2016b). AmeriFlux BASE US-Ne3 Mead - Rainfed maize-soybean rotation site, Ver. 11-5 [Dataset]. AmeriFlux AMP. https://doi.org/10.17190/AMF/1246086
Suyker, A. (2023). AmeriFlux BASE US-Ne2 Mead - Irrigated maize-soybean rotation site, Ver. 11-5 [Dataset]. AmeriFlux AMP. https://doi.org/10.17190/AMF/1246085
Wood, J. (2021). Lianhong Gu AmeriFlux BASE US-MOz Missouri Ozark Site, Ver. 9-5 [Dataset]. AmeriFlux AMP. https://doi.org/10.17190/AMF/1246081